Optical Properties and Ablation of Ophtalmic Media and Biocompatible Materials in view of Phototherapeutic Keratectomy (PTK)

Master´s Thesis by
Jens Ingemansson

Lund Reports on Atomic Physics, LRAP-225
Lund, October 1997

This thesis was executed at the Swiss Federal Institute of Technology
in Zuerich and
it was submitted to the Faculty of Technology at Lund University
in partial fulfilment of the requirements for the degree of
Master of Science in Engineering

Abstract

Rough corneal surfaces may be smoothed by performing superficial ablation, Phototherapeutic Keratectomy, with the 193 nm ArF excimer laser. In order to smooth an irregular surface a substance must be used during ablation to protect low corneal areas, so that high areas are preferentially ablated. A PMMA-disc with milled patterns was developed and used as a model for the rough cornea. This model was used to compare the ablation properties of 14 different substances used as so called Masking Agents. Further, the optical properties like attenuation, scattering and reflectivity were investigated and the attenuation coefficients and refraction indices determined. Finally, the ablation properties was compared with the attenuation coefficient. The expected correlation between ablation and attenuation was, however, not found. Preliminary results indicates that Oxane may be the most efficacious Masking Agent.

Contents

1. Introduction

The eye of the human has as outermost window open to the world, a thin structure, 0.55 mm thick called the cornea. It consists of several layers - the epithelium, the Bowman's membrane, the stroma, the Descement´s membrane and the Endothelium. The cornea is responsible for approximately 2/3 of the refractive power of the eye. For this reason, reshaping the cornea is a method widely used in an attempt to correct ametropia (refractive error of the eye)

In 1983, Trokel et. al.[1] introduced the pulsed ArF 193 nm excimer laser as a prospective tool in corneal surgery, but first 1988 it was used in investigations involving humans[2]. The excimer laser is capable of ablating the cornea with a rate of 0.24 to 0.28 μm per pulse, with minimal damage to the surrounding tissue.[3] This makes the 193 nm excimer laser to an excellent cutting instrument for corneal surgery. Presently, the ArF laser is mainly used to correct myopia (near-sightedness)[4]. This is done by ablation of a corneal volume, thicker in the corneas middle part than at the edges. The resulting flatter cornea may give a sharp visual image. This is called Photo Refractive Keratectomy (PRK).

The cornea, however, is a delicate biological tissue, for which any change in its structure, changes its transparency. In such cases the sharp vision may be lost. The change of the corneal structure may be due to e.g. corneal dystrophies (lack of nutritive substances), corneal scars (postinfectious or posttraumatic) or Salzman's degeneration[5], see example in Fig. 1.1.

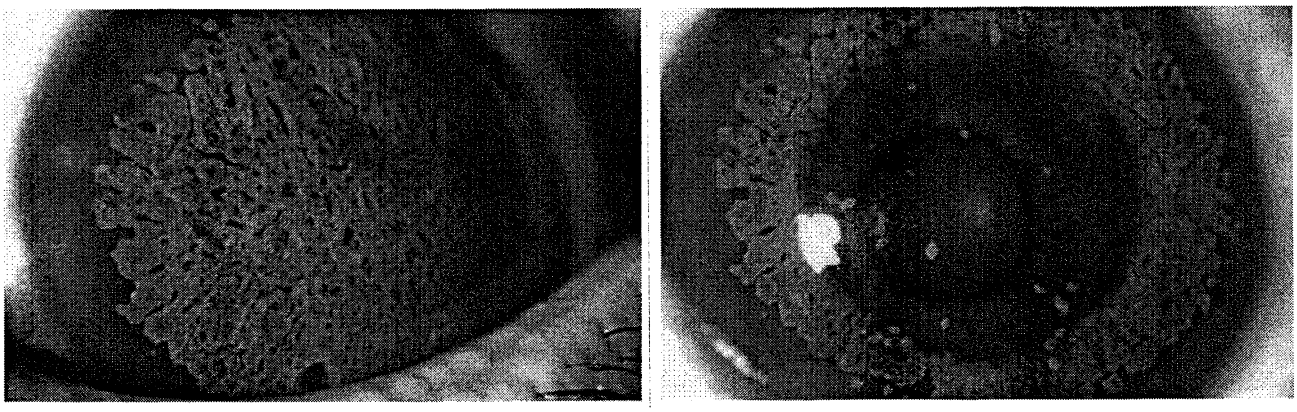

Figure 1.1 An example of irregularities on an eye. To the left before operation and to the right after operation.

[1] Torkel SL, Srinivasan R, Braren B, Excimer laser surgery of the cornea, *Am J Ophtalmol,* **96**, 715-720, 1983.
[2] Stark WJ,Chamon W, Kamp MT et al., Clinical follow up 193 nm ArF excimer laser photokeratectomy, *Ophtalmology*, **99**, 805-811,1983
[3] Fantes FE, Hanna KH, Waring III GO, et al., Wound healing after excimer laser lamellar keratectomy, *Ophtamology,* **96**, 654-664, 1989
[4] Christopher JR, Excimer laser phototherapeutic keratectomy, *Int. Ophtalmology Clinics*, **36**,127-136,1996
[5] Dimitri TA, et al., Phototherapeutic keratectomy, the VISX Experience, *Corneal Laser Surgery*, p.213-226,1995

If these changes in the structure are irregularities located at the surface or in the anterior third of the cornea, it may be possible to treat the patient by removing the irregular structure.[6] The treatment is often performed invasively by mechanical methods, e.g. lamellar or penetrating keratoplasties. With excimer laser ablation, the same operation may be done non invasively.[7] This kind of treatment with laser ablation is called Photo Therapeutic Keratectomy (PTK).

The irregularities can be smoothed using varying spot size or through rotation of the patients head (!!)[7]. Present delivery system are operated on the basis of a variable but rotationally symmetric mask (iris diaphragm, rotating mask or ablatable mask). New laser delivery systems, using a focused spot of 0.5 to 1.0 mm are currently under development. However, at this time only large uniform beams, with a diameter up to 90 mm, are available for PTK treatments. As a result irregularities can not, with present technique, be levelled only through control of the laser. The irregularities will just be repeated on a lower level, as shown in Fig. 1.2.

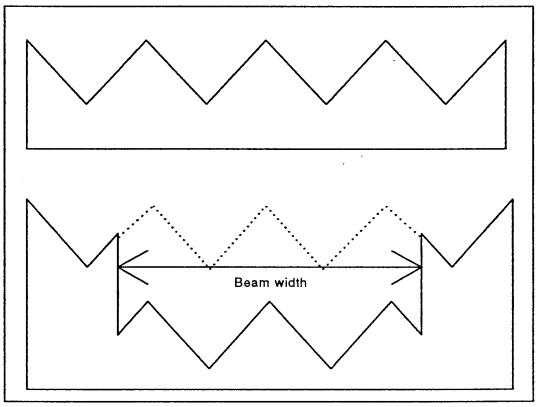

Figure 1.2.
Above: Irregular initial surface
Below: Surface after laser ablation

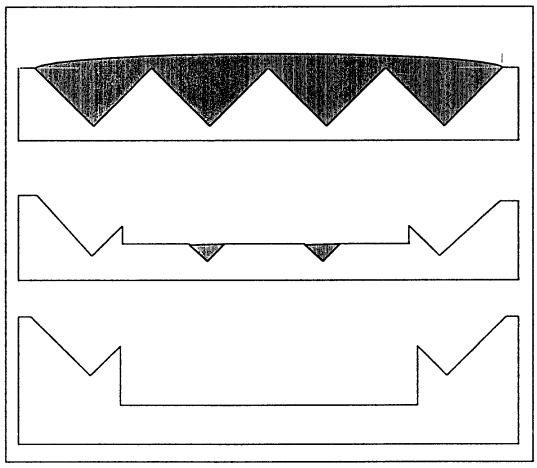

Figure 1.3.
Above: Irregular initial surface, filled with liquid (masking agent)
Middle: Theoretical surface, during the ablation
Below: Theoretical surface obtained after laser ablation.

If the irregularities at the surface are filled with a liquid having the same ablation properties as the cornea, a smoother surface can theoretically be obtained, as shown in Fig. 1.3.

Such liquids are commonly refered to as smoothing agents, masking agents, modulation liquids, corneal modulators or ablatable masks. In the following, they will be referred to as masking agents.

Prior to this work, comparative studies have already been published by Fitzsimmons and Fagerholm[8] as well as by E.W. Kornmehl et al.[9] These works compared three different masking agents each, non of which was the same in both. A number of other liquids have been used for

---

[6] Dimitri TA, et al, p. 214
[7] Dimitri TA, et al, p 235
[8] Fagerholm P., Fitzsimmons T.D., Superficial keratectomy with the 193 nm excimer laser, *Acta Ophthalmologica,* **69**, 641-644, 1991.
[9] Kornmehl EW, et al., A comparative study of masking fluids for excimer laser PTK, *Arch Ophtalmol*, **109**, 860-863, 1991

PTK as masking agents. However, their adequateness for the purpose of PTK has not yet been proved. Moreover, an easier, more accurate and absolute method to determine the ablation properties of the liquids is desirable.

1.1 Subject

It is assumed that the optical properties are closely related to the ablation properties of a material. Therefore the purpose of this work consists of, in a first stage, measuring the optical properties of various masking agents used in PTK, attenuation coefficient, refraction index etc, and, in a second stage, of developing a method to determine the corresponding ablation rates. For this purpose, the various measurement methods that are currently used for the visible or near UV range have to be analysed and implemented for the far UV region, down to the ArF excimer laser at 193 nm. In addition, the influence of the wavelength should be determined to evaluate the potential of other lasers not yet in use such as, e.g., the newly developed 5f-Nd: YAG laser (213 nm). This laser displays potential advantages for ophtalmic ablation (lower costs, lower running costs, higher modularity etc.).

2. The Masking Agents

The masking agents used are displayed in table 2.1. The most volatile liquids are listed first, e.g. perfluorooctane, and the more viscous, e.g. Oxane, follow below. The liquids containing silicone, which are not used in the ablation experiments in Ch. 4 (they can damage the instruments), are listed separately at the end.

Name	Main Substance	Producer	Comments
Perfluorooctane	100%	Adatomed GMBH, Munich D	fluorinated
Perfluorodecaline	100%	Opsia	
Distilled water			
NaCl 0.9 %	0.9 % NaCl solution	Lab. Dr G. Bischel AG, Interlaken CH	
BSS	balanced salt solution	Alcon, Pharma-ceuticals Ltd, ZG.	
Tears Natural	0.3 % Methyl-hydroxypropylcellulosum + 0.1 % Dextranum-70	Alcon	
Tetracaine	1 % Tetracaini hydrochloridium	CIBA Vision AG, Niederwang. CH	
Dextran 7%	15 % Dextran diluted with sterile BSS		
Dextran 15 %	15 % Dextran solution		
Methocel	2 % Methylhydroxy propylcellulosum	CIBA Vision AG	
Celluvisc	1 % Carboxy-methylcellulosum natricum	Allergan AG, Lachen CH	
Healon	1 % Natrium Hyaluronate	Pharmacia	
Ophthalin	Hyaluronate preparation	Ciba Vision AG	

Table 2.1a. The different liquids used

Oxane	Pure silicon oil	Opsia	
DDS	75 -78 % Dimethyl 22 - 25 % Diphenyl - siloxane	Petrarch Syst.	viscosity (ctsk) = 1000 - 2000
Silol 5000	Silicone Oil	Adatomed GMBH	viscosity = 5000 cps
PTS	Polymethyl - 3.3.3 - Trifluoropropyl siloxane	Petrarch Syst.	viscosity (ctsk) = 100 000

Table 2.1b. The liquids containing silicon.

3. Absorption and Scattering

3.1 Theory

Light is a electromagnetic wave, that may be described by its complex electric field, E. This wave propagates along the axis z in a medium which may be characterised by its complex index of refraction, n + iκ.[10]

$$E = E_0 e^{+ikz} = E_0 e^{+\frac{i2\pi}{\lambda_0}(n+i\kappa)z} = E_0 e^{\frac{i2\pi}{\lambda_0}z} e^{-\frac{2\pi\kappa}{\lambda_0}z} \tag{3.1}$$

Light intensity, I, which is proportional to EE^* can be derived as:

$$I = E_0^2 e^{-\frac{4\pi\kappa}{\lambda_0}z} \tag{3.2}$$

writing $$\mu_a = \frac{4\pi\kappa}{\lambda_0} \tag{3.3}$$

results in $$I = I_0 e^{-\mu_a z} \tag{3.4}$$

This is known as the Lambert-Beer law, where μ_a is the absorption coefficient. On a macroscopic basis, this can be derived, assuming that in a slice, dz, a constant proportion of the incoming intensity is locally absorbed:

$$dI = -\mu_a dz \tag{3.5}$$

Integration of eq. (3.5) gives eq. (3.4).

Using the same philosophy, a part of the light may also be lost by scattering. A scattering coefficient μ_s is used, so that in terms of scattering (like absorption):

[10] Bergman, Schaefer, Lehrbuch der Experimentalphysik, Band 3 (Optik), Walter de Gruyter, 1989

$$I = I_0 e^{-\mu_s z} \tag{3.6}$$

When both scattering and absorption are present, it may be helpful to write the total attenuation coefficient, μ_t , as:

$$\mu_t = \mu_a + \mu_s \tag{3.7}$$

When light strikes matter, several processes are started. Through these the photons can be reflected, scattered or absorbed.[11] Conservation of matter gives:

$$I_0 = I_T + I_S + I_A + I_R \tag{3.8}$$

Here I_o is the incoming light, I_T the transmitted, I_S the scattered, I_A the absorbed and I_R the reflected radiation.

Transmittance, T, is defined as I_T / I_0 , reflectance as I_R / I_0. Absorbance, however, is defined from transmittance:

$$A = -\log_{10} T \tag{3.9}$$

3.1.1 Absorption

Absorption originates at the atomic level and therefore the light has to be seen as photons, concerning absorption. The wavelength associated with the photon corresponds to its energy through $E = hc/\lambda$.

Absorption generally arises from movements of the electrons in the atoms or molecules from which a substance is built. The electrons in molecules can, strongly simplified, move between three kinds of energy levels: rotational, vibrational and electronic. Rotational levels represents the levels with the smallest energy gaps and the electronic levels the ones with the largest. UV-photons are highly energetic and may cause jumps between the electronic levels.[12]

3.1.2 Scattering Processes

Scattering actually is not one but many different processes: elastic scattering, with conservation of the wavelength, like Mie-, Resonance-, Thomson- and Rayleigh- Scattering and inelastic scattering, with change of the wavelength, like Compton, Raman and Brillouin Scattering.[13]

---

[11] Sommer L., Analytical Absorption Spectrophotometry in the visible and the UV - The Principles, (Studies in Analytical Chemistry) , Elsevier, Amsterdam, p.13, 1989.
[12] Svanberg S, Atomic and Molecular Spectroscopy, Springer Verlag, Berlin-Heidelberg,, 56-60, 1992.
[13] Ishimaru A, Wave Propagation and Scattering, London, 814-815, 1991

Rayleigh Scattering arise when light interacts with a particle, such as a molecule, smaller than the wavelength of the light. This results in weak radiation of the same frequency as the incoming radiation. The intensity of this radiation is proportional to the fourth power of the frequency [14] .

$$I_S \propto \frac{1}{\lambda^4} \tag{3.10}$$

Therefore the Rayleigh is 256 times larger at 200 nm then at 800 nm. Hence, the scattering can be large at short wavelengths even though negligible scattering can be seen at longer wavelengths.

3.1.3 Influence of Interfaces

Determination of the attenuation coefficient is difficult because transmission is often mixed with border effects occurring at interfaces. Example of a thin plate, where multiple internal reflection occur is displayed in Fig. 3.1

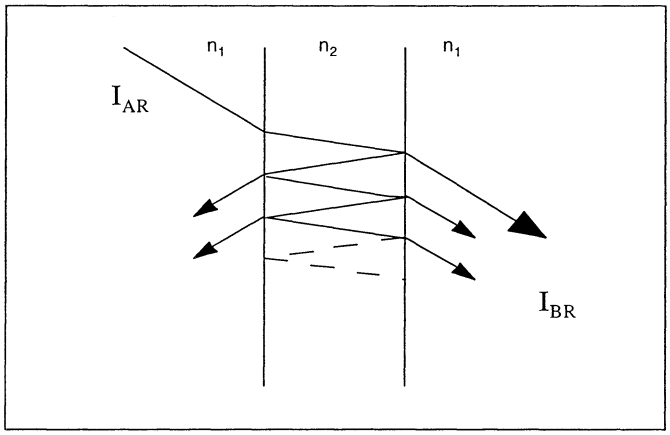

Fig.3.1. Reflection of an incoming light beam in the interfaces between two media

A theoretical analysis of the behaviour of a light ray through a thin plate is accomplished in appendix A. Eq. (A.8) describes the theoretical transmittance through the interfaces in fig. 3.1. under the assumption of no occurring absorption.

$$T_w = \frac{I_{BR}}{I_{AR}} = \frac{1-R}{1+R} \tag{A.8}$$

With no scattering present, the reflectance R of an interface between two media is composed only of the specular reflection. It is governed by the Fresnel law:

[14] Svanberg S, 56-60

$$R = \frac{(n_1 - n_2)^2}{(n_1 + n_2)^2} \qquad (3.11)$$

However, the refraction index, n, is a function of the wavelength. The dispersion of n with the wavelength, can be estimated through the Abbe constant, ν.

$$\nu = \frac{(n_D - 1)}{(n_F - n_C)} \qquad (3.12)$$

Here, n_D, n_F and n_C are the refraction indices at 589, 486 and 656 nm respectively.[15]

3.2 Instrumentation

This part contains a technical as well as a qualitative description of the different instrumental systems, which were used in the experiments.

Following instrumentation systems were used for the measuring of absorption and scattering of UV-radiation:

a) Two dual beam spectrophotometers from two different manufacturers, used with following accessories:

a1) QS - cells.

a2) An integrating sphere.

a3) A external fibre optic path.

For the determination of the refraction index, n, and the Abbe constant, ν

b) An Abbe refractometer

was used

[15] Abbe Refractometer, Carl Zeiss, Instruction Manual.

3.2.1 The Spectrophotometer

Two dual beam spectrophotometers were used. The first one, a model UV-1601 (Shimadzu), has a design as shown in Fig. 3.2 [16]

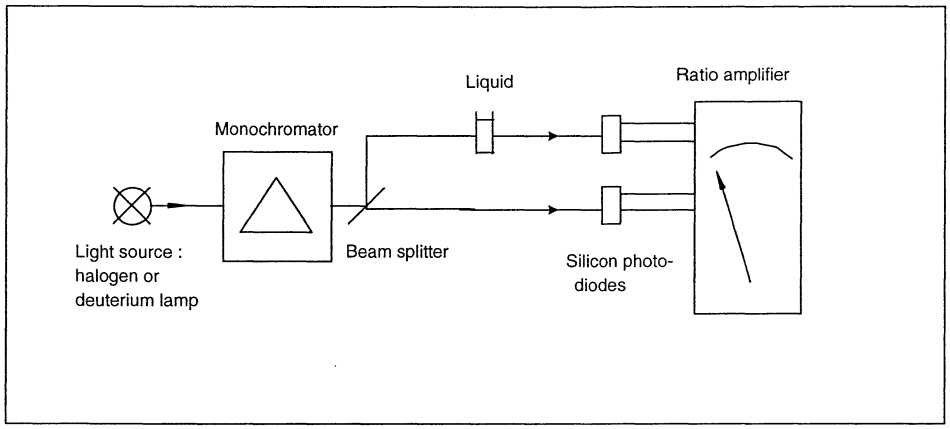

Fig. 3.2. The basic design of the UV-1601 spectrophotometer.

A second dual beam spectrophotometer, a model Lambda 6 (Perkin-Elmer) was also used. This instrument has basically the same design as the Shimadzu. The differences are above all that Lambda 6 has a photomultiplier as detector and that it has adjustable slit width and response (integration) - time. The former should give better linearity and signal to noise ratio to the spectrophotometer than the Si-detector in the Shimadzu and the latter makes it possible to optimise the resolution / signal-to-noise relation.

The manufacturers specifications are as follow in Table 3.1.

[16] Shimadzu UV-1601, Instruction Manual, Shimadzu Corp.

	Shimadzu UV-1601[17]	Perkin Elmer Lambda-6 [17]
Spectral Band Width	2 nm	0.25, 1, 2, 4 nm @ 656.1 nm
Wavelength Accuracy	± 0.5 nm	± 0.3 nm
Wavel. Repeatability	± 0.1 nm	± 0.1 nm
Photometric Accuracy	A = 1.000 ± 0.004 A = 0.500 ± 0.002	A = 1.000 ± 0.005 measured with NBS 930 filters
Photometric Repeatability	A = 1.000 ± 0.002 A = 0.500 ± 0.001	A = 1.000 ± 0.001 measured with NBS 930 filters
Baseline Stability	ΔA < ± 0.001 / h.	ΔA < 0.0005 / h. At 340 nm, 4 nm SBW, 6 respons time.
Stray light	< 0.05 %	< 0.02 % @ 220, 340, 370 nm, 2 nm SBW, 5 respons time
Noise Level	ΔA = 0.002	ΔA < 0.0003 @ 500 nm, 0 A, 4 nm SBW, 6 respons time
Light Source	50 W halogenlamp or Deuteriumlamp	Tungsten- or Deuteriumlamp
Detector	Silicon Photodiode	Photomultiplier
Monochromator	Aberration correcting concave blazed holographic grating	Holographic grating monochromator

Table 3.1 Specifications for Shimadzu UV-1601 and Perkin Elmer Lambda-6

Accuracy

The wavelength accuracy of the instruments was checked with a holmium glass filter. The holmium glass filter has a spectrum with narrow peaks for the wavelengths in table 3.2.

Table 3.2 shows the measurements made with the holmium filter with both instruments.

[17] Perkin-Elmer, User manual.

Should be, λ (nm)	Shimadzu UV-1601	Perkin Elmer Lambda-6
241.5 ± 0.2	241.0	---
279.4 ± 0.3	279.3	278.9
287.5 ± 0.4	287.8	287.3
333.7 ± 0.6	334.2	333.6
360.9 ± 0.8	360.8	360.5

Table 3.2 Wavelength accuracy made with Holmium glass filters at 540 nm after warm-up.

Considering the specified accuracy error of maximum 0.5 nm and 0.3 nm for the Perkin-Elmer and the Shimadzu, respectively, the accuracy errors are too large for the Lambda-6. They are also growing towards shorter wavelengths.

The photometric accuracy was checked with a few different grey filters. A grey filter is a glass filter with a certain absorption at a certain wavelength, normally 540 nm. Table 3.3 shows the photometric accuracy at $\lambda = 540$ nm. Two measurements with each filter and spectrophotometer were made and an average value calculated.

The photometric accuracy error for the absorbance was for the Perkin Elmer never higher than the specified ± 0.005, whereas the Shimadzu exceeds the stipulated 0.500±0.002 resp. 1.000±0.004. To be noted is that these measurements were made at $\lambda = 540$ nm and not at around 200 nm.

Should be, A	Shimadzu UV-1601	Perkin Elmer Lambda-6
0.204	0.199	0.203
0.597	0.600	0.598
1.210	1.211	1.206
1.747	1.750	1.744

Table 3.3. Photometric accuracy after warm-up at $\lambda = 540$ nm

Stray-light, i.e. radiation of wavelengths outside the narrow band ideally transmitted by the monochromator, depends on many factors. These includes the sample itself, light intensity, slit width and -height, light leaks etc. In a well designed diffraction grating monochromator, almost all the stray-light originates from the grating [18].

The two spectrophotometers used in the experiments were both equipped with holographic gratings, involving less stray-light than ruled (mechanically produced) gratings. For the Perkin-

[18] Burgess C.and Knowles A, Standards in Absorption Spectrometry (Ultraviolett Spectrometry Group), Chapman and Hall, London, 95-99, 1981

Elmer device the stray-light was specified to less than 0.02 % at λ = 220 nm, while for the Shimadzu it was said to be less than 0.05 % (wavelength unspecified).

In the UV region just around 200 nm, following factors probably make the stray-light higher than the specified values above. [19]

a) Below 250 nm the reflectance of the aluminised mirrors in the spectrophotometer is liable to deteriorate with time. Because most of the stray-light in the region below 250 nm is of higher wavelengths, the proportion of the stray-light is likely to increase with time.

b) If the absorption of the samples is higher for wavelengths around 200 nm than for longer wavelengths, there will also be an increase of the stray-light proportion.

c) The absorption by air becomes important below 200 nm, which, as well as the two previous factors, will increase the stray-light proportion.

If the analysis is restricted to point b) above, i.e. the influence of the sample, the relation between apparent and true absorption, can be calculated.

If all the stray-light is assumed to be transmitted by the sample, i.e. the stray light is assumed to originate from wavelengths with no absorption by the sample, equation (3.13) can be derived.[19]

$$A' = -\log_{10} [\, 10^{-A} (1-s) + s \,] \qquad (3.13)$$

Here A' and A are the apparent and true absorbance of the sample respectively. s is the stray light rate of the incoming light. If one percent of the incoming light is stray light, s becomes 0.01. If the specifications for the stray light in the spectrophotometers are reliable, Eq. (3.13) will give a deviation for the Perkin-Elmer (s = 0.02 %) of - 0.027 at A = 2.500 and for the Shimadzu (s = 0.05 %) of - 0.064 at A = 2.500 . To be observed is that these deviations do not include point a) and c) above. However, the effects from point b) are possibly overestimated because some of the stray-light is most likely absorbed by the sample.

Repeatability

Repeatability consists of two components: photometric repeatability, mainly depending on the detector and wavelength repeatability originating from the adjustments of the grating.

For a spectrophotometer with a photomultiplier as detector, like the Lambda - 6, the photometric repeatability is worst at very short and very high absorption. This is a consequence of variations of the electron current arising from the electron emitting surface of the photomultiplier. When very few photons (high absorption) strike the surface, very few electrons are emitted, resulting in repeatability errors. When very few photons are absorbed, the ratio of the intensities of the two beams, is near 1, what makes the exact determination of the ratio difficult. [19]

---

[19] Meister E., Spectrophotometri, Instruktion fuer Physikalisch Chemisches Praktikum 1,1997

The wavelength repeatability is the other reason for repeatability errors. Especially when the absorption increases strong with the wavelength, the wavelength repeatability may cause errors.

As a result of these findings and the problem with stray-light for high absorption, absorption measurements have been suggested to stay between 0.05 and 2.0 A.[20]

With an empty Quartz-suprasil (QS)-cell, the over all repeatability at 193 and 213 nm were checked for the two spectrophotometers. To test the repeatability accurate, the wavelength were set both from longer and shorter wavelengths. This means that possible play in the mechanism would have been discovered. For the 20 measurements at each wavelength, the total repeatability error never exceeded 0.003 A for any of the two spectrophotometers

3.2.2 The Cells

Because the interest of this study lies in the deep UV-region, adapted measurement cells should be chosen. For that purpose, various material are commercial available (Fig. 3.3). QS-cells are the cells with the slightest absorption for wavelengths on the vacuum UV border (200 nm) and were therefore used in this work.

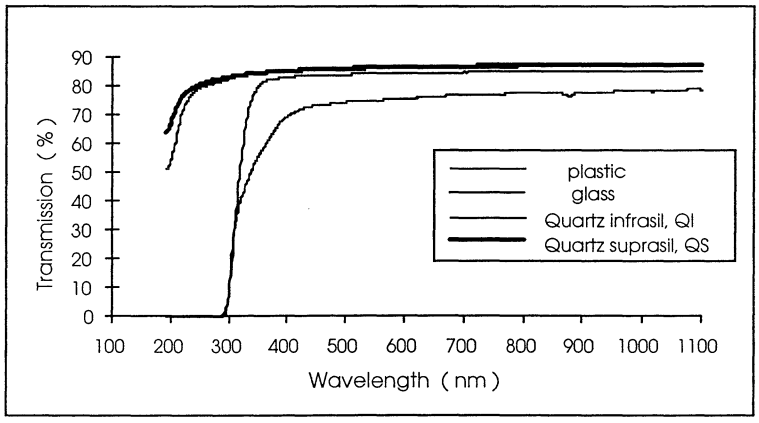

Fig. 3.3 Four kind of cells compared. The QS- cell has the highest transmission at short wavelengths.

As discussed for theoretical interfaces in Ch. 3.1.3, multiple internal reflections may cause deviations between true and apparent transmittance. An practical example of two interfaces, surrounded by media with negligible attenuation, is a cell wall in air. The equation for the transmittance becomes the same as in the theoretical case, Eq.(A.8) (Appendix A). For an empty cell, the theoretical equation for four interfaces in Appendix A may be usable:

$$T_C = \frac{I_{BR}}{I_{AR}} = \frac{1-R}{1+3R} \qquad \text{(A.10)}$$

Here I_{BR} is the light transmitted through the cell and I_{AR} the incoming light. A filled cell is theoretical described through Eq. (A.16) in Appendix A:

[20] Sommer L., p.95

$$T_{FC} = \frac{I_{BR}}{I_{AR}} = \frac{(1-R_0)^2(1-R_1)^2 e^{-\mu L}}{(1-R_0R_1)^2 - (R_1 + R_0 - 2R_1R_0)^2 e^{-2\mu L}} \qquad \text{(A.16)}$$

Here the denominator describes the influence from multiple internal reflection. The maximum error, caused by multiple internal reflection in a filled cell can be estimated to < + 2 % transmittance what is equal to < - 0.009 in absorbance.

The path lengths of the cells has a tolerance of ± 1.0 % [21]. If the absorbance is 1.0, this may cause an error in the measured absorbance of up to 0.01.

The angle of the cell normal against the beam cause errors. An angle deviation of 3° causes a systematic error in the absorbance with the magnitude 0.001 .[22]

3.2.3 The Integrating Sphere

An integrating sphere is used as an accessory to a spectrophotometer. It collects the scattered light from a sample, so that the absorption instead of the attenuation of the sample can be measured.

The integrating sphere principally works in accordance with Fig. 3.4 below.

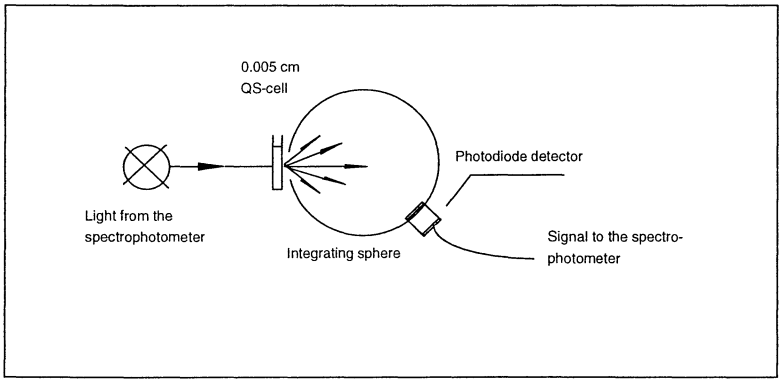

Fig 3.4 The principle of the integrating sphere.

In the experiments a model RSA-SZ-1601 (Labsphere) was used. It is an optical bench which includes transfer optics and a two inch diameter integrating sphere and it's designed for the Shimadzu UV-1601. The sample beam of the spectrophotometer is led through the sample into the integrating sphere, while the reference beam is not influenced from any new object. The sphere is coated with Spectralon which has a reflectance factor, according to the manufacturer's specifications, higher than 0.95 from λ = 350 nm to λ = 2400 nm.[23]

To check the reflection below 350 nm, the reflection from a spectralon sample was measured with the external fibre optic system described in Ch. 3.2.4, see Fig 3.5.

[21] Hellma Kuvetten, Hellma GmbH, Germany.
[22] Burgess C. and Knowles A., p.7
[23] Labsphere, Instruction manual for RSA-SZ-1601,1989

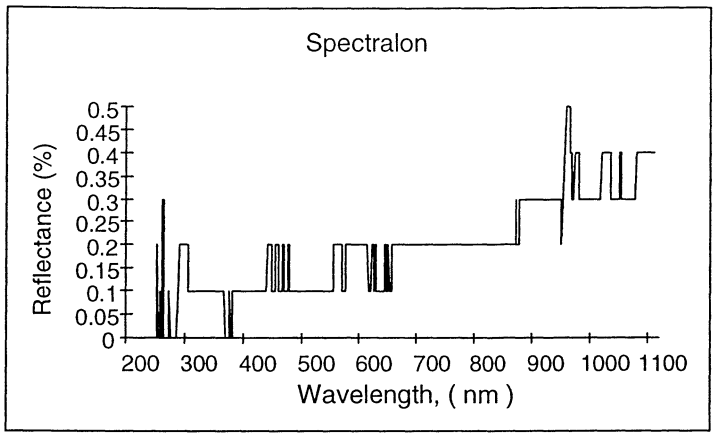

Fig 3.5. The reflectance in percent for a spectralon sample.

The low reflectance measured, is due to the diffuse spreading of the light striking the spectralon sample. The for the experiments interesting wavelengths, 193 and 213 nm, has no, with this system, measurable reflection. First at around 250 nm there is any reflection at all, indicating that measurements below 250 nm will be difficult.

To improve the system, a metal screen with a transmittance of 2.4 % was placed in the reference beam. Due to the increase of the ratio of the two beam intensities in the model UV-1601, the photometric precision was improved. [24]

3.2.4 The External Fibre Optic Path

To measure the angle dependence of the scattering, an external system according to Fig.3.6 was produced.

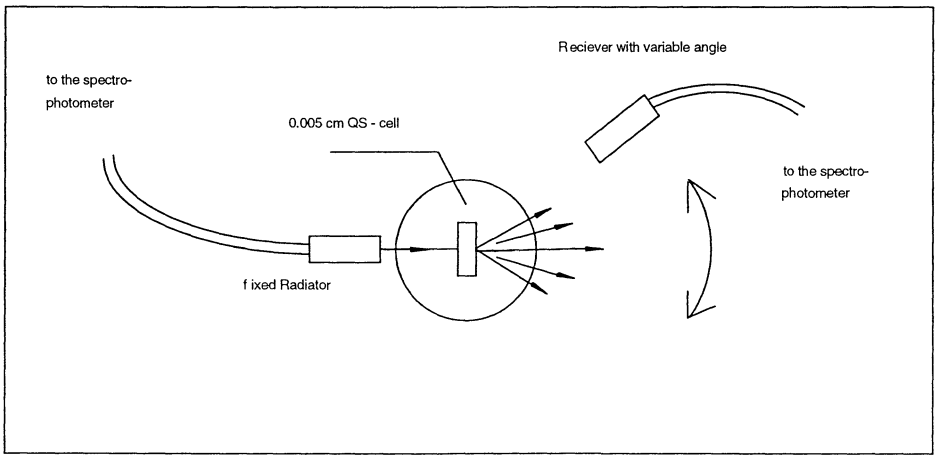

Fig 3.6 The basic design of the external fibre optic path

[24] Burgess C. and Knowles A, p.88

The angle between the radiator and the receiver can be arbitrarily adjusted. In this setup only light scattered within the cell is detected, resulting in much smaller signals then in the spectrophotometer. The light is transported through a quartz-fibre to a light conductor placed in the cell holder of the spectrophotometer. All radiation do not strike this light conductor and all energy, passing through the system and coming out on the other side of this conductor do not strike the photocell. Moreover there are losses in the fibre itself. Therefore the effect transmitted through the fibre is less then the effect hitting a cell directly placed in the spectrophotometer. Additionally, this system loses effect between the source and receiver at the ends of the fibres as a result of the spreading of the light from the fibre ends. This happens in spite of the focusing quartz-lenses mounted on the ends of the fibres.

The approximately relation between effect transmitted, without sample, directly in the spectrophotometer and effect guided through the fibre optic path is shown in Fig. 3.7. The effect passing through the fibres was measured both for a single fibre and for two fibres with the end parts directed right against each other to ensure maximum coupling.

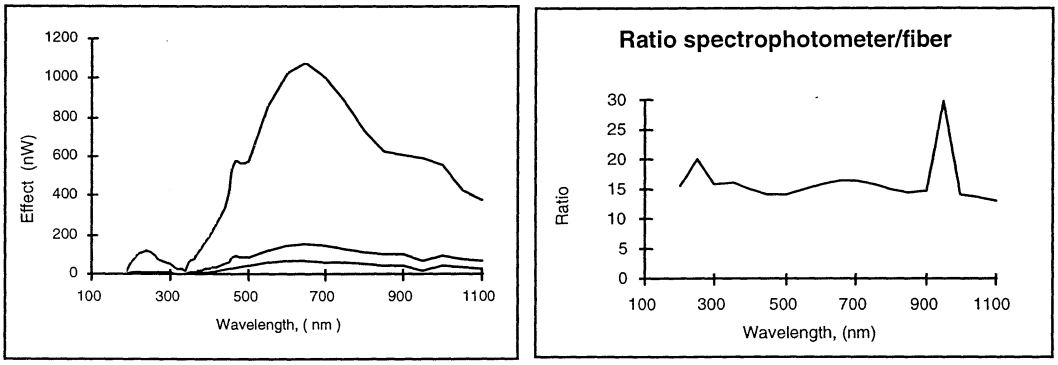

Fig 3.7. In the figure to the left, the uppermost line is the effect measured direct in the spectrophotometer. The middle line is the effect passing through one fibre and the lowest, the effect passing through both fibres. In the figure to the right, the ratio of the effect measured direct in the spectrophotometer and the effect passed through two fibres is presented.

The measurements were made with a photodetector (Si-photodiode) with a quartz window enabling measurements in the deep UV-region down to 190 nm (Newport Corporation model 818-UV). The detector was attached to a digital meter, model 835, which is able to measure power values down to 1pW.[25] This model is not calibrated below 250 nm though it is possible to measure below that wavelength. As a consequence the curves in Fig. 2.8 are not calibrated below 250 nm. The energy flowing through the fibres is less than one tenth of the energy directly transmitted (see Fig. 3.7).

The external fibre optic system was used together with the Shimadzu UV-1601. To get best possible precision the Newport model 818-UV together with model 835 were used as detector instead of the built-in photodetector.

[25] Newport Corporation, Model 835 Operating Manual, Newport Corporation, Fountain Valley, U.S.A, 1987.

3.3 Methods

This chapter describes the methods used with the different systems introduced in the previous chapter 3.2. Further it tries to motivate the choice of these particular methods.

3.3.1 Measurements with the Spectrophotometer

Spectrophotometer measurements where made with the purpose to obtain most accurate values for the attenuation coefficients of the different samples.

Three possible methods to measure the attenuation in a spectrophotometer were analysed.

a) The simplest way is to place the cell containing the media to be measured, in the sample beam and to not place any cell in the reference beam. The attenuation could then be theoretically calculated through equation (A.16) in App. A.

b) Another method is to use two cells of different thickness of which one is placed in the reference beam and one in the sample beam. Hence, the attenuation that is measured doesn't need to be corrected through calculations.

c) A last method is to make a number of measurements like the one in a) but using cells with different path lengths each time. If the sample follow the Lambert Beer-law, a plot with the absorbance as function of the path length should theoretically, the denominator in (A.16), corresponding to the multiple reflections, disregarded, become a straight line.

Due to poor accuracy of the known values of the refraction indices, method a) is difficult to use for accurate measurements. Alternative b) should be a good method if the absorbance for only one pathlength is to be determined. The advantage of method c) is that with this method, the assumed agreement with Lambert Beer-law could be investigated.

From the two most accurate methods, b) and c), the latter alternative was chosen. Above all because of the possibility to check the values against the Lambert Beer - law.

Although not as important as in method a), because of e.g. the multiple reflections, see Eq. (A.16), the reflectance for the interface between the cell and the masking agent is also in method c), interesting to know. The reflectance may be calculated through the Fresnel law, Eq. (3.12). Therefore, with an Abbe Refractometer, the refraction index, n, and the Abbe-constant, ν, was measured. From these variables, the refraction indices at 193 and 213 nm can be roughly estimated.

Choice of Spectrophotometer and Slit Width

From the two available spectrophotometers, the Perkin-Elmer Lambda-6 instrument was chosen. The main reasons for this choice were:

- Higher photometric linearity, due to the photomultiplier[26](the Shimadzu instrument has a photodiode as a detector).
- A, according to the specification, better accuracy and repeatability, and
- the possibility to adjust the slit width which determines the Spectral Band Width (SBW) .

In Fig. 3.8, the absorbance by an empty QS- cell is plotted as a function of the SBW.

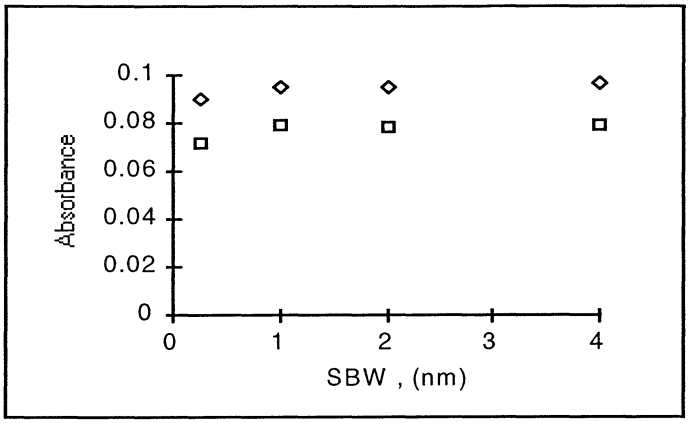

Fig 3.8. Absorbance as a function of the SBW for a empty QS - cell. The turned squares shows the absorbance at 193 nm and the normal squares at 213 nm.

With a too narrow SBW, the signal to noise ratio (SNR) will be too low and with a too broad SBW, the sensitivity for peaks and other irregularities in the attenuation spectra, will be too low.[27] The attenuation spectra for the masking agents were not expected to vary strong with the wavelength. As a consequent and with regard to Fig. 3.8, the SBW was chosen large, to 2 nm, to maximise the signal to noise ratio.

The Cells

In accordance to method c), measurements with cells of four different path lengths were made. The path lengths: 0.001, 0.005, 0.01, 0.02 cm were used. For the two wavelengths, 193 and 213 nm, each masking agent was measured twice. The agents were put in the cell with a sterile injection syringe. The cells were always carefully placed in the same position and with the same side against the light beam.

To get the cells clean is a problem working with spectrophotometry. Especially in the almost vacuum-UV it is time consuming to get the same transmission between two measurements. The best way, found, to clean the cells was to gently polish them with optical ethanol (or optical acetone for the silicon-based substances) and lens tissue. When stronger cleaning was needed, a basic liquid (Hellmanex from Hellma) was used. Goddard[28] suggests optical ethanol and the use of a ultrawave bath to achieve best possible results. With this method he achieved transmittance-

[26] Svehla G., Comprehensive Analytical Chemistry, **4**, Elsevier, Amsterdam, p.69, 1975
[27] Burgess C. and Knowles A., 9-10
[28] Goddard D.A., The Cleaning of vitreous silica cells, *UV Spectrometry Group Bulletin*, **4**, 19, 1976

values for a single cell-wall, equalling or even exceeding the theoretical ones. However, the transmittance achieved from the method used in the experiments did not differ too much from those achieved by Goddard and in addition, a lot of time was saved.

To measure the repeatability of the cleaning of the cells, a 1mm QS-wall was used. 20 measurements at 193 nm with each spectrophotometer were made. The Perkin-Elmer-instrument brought an average of 88.4 % with a max. deviation of 0.4 %. The corresponding figures for the Shimadzu were 87.7 % and 0.8 %.

Attenuation coefficient

The measured absorbances were plotted in Absorbance vs. Path length diagrams and linear regression was used to calculate a straight line through the points. According to the equation for light propagating through a cell in Ch. 3.2. (Eq. A.16), the attenuation coefficient can be calculated from the slope of the straight line. The absorbance is a $\log_{10}$ - function of the transmission, while the attenuation coefficient is a ln - function. To get the attenuation coefficient, μ_t, the calculated slope therefore was divided with log (e) = 0.434.. . The measured absorbances were used for a statistical analysis. A 95 % confidence interval was calculated for μ_t from the t-distribution and the linearity was estimated through calculations of the r^2 - values.[29]

3.3.2 Measurements with the Integrating Sphere

The measurements with the integrating sphere were aimed to show in what extent the attenuation coefficients measured are a result of absorption in the materials and/or a result of scattering.

For every material a spectrum from 190 to 700 nm was measured in the Shimadzu instrument, with and without the integrating sphere. The 0.005 cm cell was used as sample cell with no cell placed in the reference beam.

3.3.3 Measurements with the External Fibre Optic Path

The external fibre optic system was used to determinate the angular dependence of the scattering.

At the two wavelengths 193 and 213 nm, for every material, the transmitted power in angles between 0° and 90° as well as the reflected energy in angles between 90° and 135° was measured. The transmittance measurements were made in steps of 1° and the reflectance measurements in steps of 5°.

[29] Kreyszig E., Statistische Methoden und ihre Anwendungen, Vadenhoeck & Ruprecht, Goettingen, 270 - 271 & 300 - 301, 1979

3.4 Results

3.4.1 Attenuation Coefficient

In Figures 3.9-10, the absorbance as a function of the path length is plotted. If the samples follow the Lambert Beer - law, the points should be on a straight line. The slope is the attenuation coefficient. However, the absorbance measured with the 0.02 cm cell often drops, especially at the wavelength 193 nm. Therefore the attenuation coefficient is calculated also for just the three first path lengths. For all masking agents, but Healon and Ophthalin, the slope of the straight line in the diagrams, arises from all four path lengths. To make the diagrams clearer, an average was calculated from the two measurements made with each sample. Hence, there is just one mark for each path length.

The results from the measurements of the direct attenuation in the Lambda-6 is presented in Tables 3.4-5. For all masking agents, but Tetracaine, the statistical analysis was made for six (two measurements per pathlength - three pathlengths) and eight (four pathlengths) measured values respectively. The slope was calculated with linear regression, using the least square fit. The tolerances for the attenuation coefficient shown in Tables 3.4-5, are 95 % confidence intervals calculated from the t-distribution. The r^2 - value also shown are a measure of the linearity of the plotted values. If r^2 equals one, all points are on the line. In the calculation of the confidence interval, the measured absorbance for each masking agents is assumed to have the same variance at every pathlength.

As can be seen in Fig. 3.10, Tetracaine attenuates too much to be measured and calculated with this normal method. The cells with a path length longer than 0.001 cm, gave a too high and uncertain absorbance. Therefore, Tetracaine at 193 nm was just measured with the 0.001 cm cell. Six measurements were made and the absorbance from the empty QS - cell was subtracted from each measurement. An average and a 95 % confidence interval was then calculated from the six values. This procedure will give rise to an error due to the reflection in the cell. According to the Abbe - constants and refraction indices in Table 3.6, Tetracaine can be assumed to have approximately the same properties of reflection as water. Using the optical reflection parameters of water would change the attenuation coefficient to 1770 cm^{-1}.

The refractive indices, n , at λ = 589.3 nm and the Abbe number measured with the Abbe refractometer are shown in Table 3.6 below. The refractive indices was measured with an accuracy of $\pm$ 0.0005 and for the Abbe number with an accuracy of $\pm$ 0.5.

Absorption as a function of the path length. Measured at 213 and 193 nm with each of the 16 masking agents.

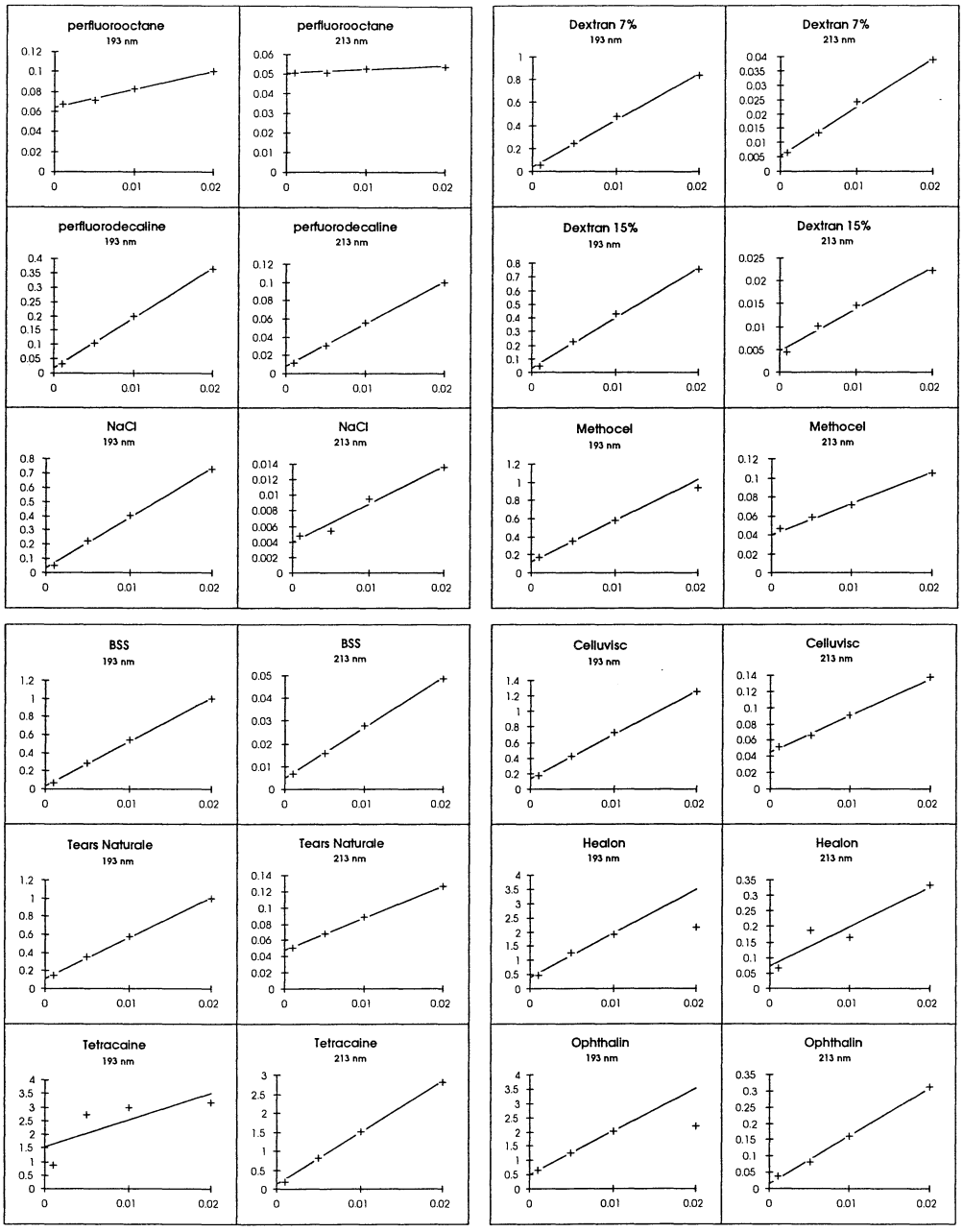

Fig 3.9 The y-axis shows the absorbance and the x-axis the pathlength of the cells.

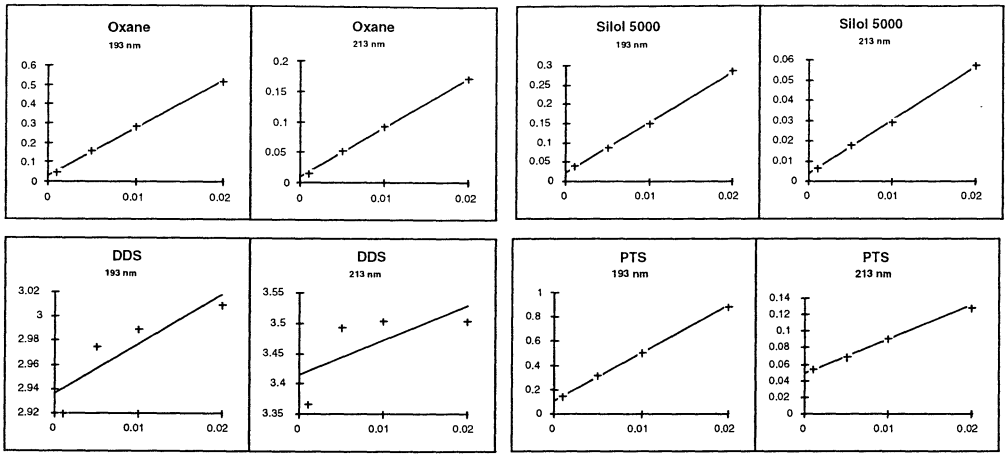

Fig 3.10 The y-axis shows the absorbance and the x-axis the pathlength of the cells.

Masking Agents at 193 nm	Att. coeff. μ_t, 3 points	r^2 - value	Att.coeff. μ_t, 4 points	r^2 - value
Perfluorooctane	4.46 ± 1.17	0.966	4.32 ± 0.39	0.992
Perfluorodecaline	42.5 ± 2.9	0.998	40.2 ± 2.0	0.997
NaCl	91.2 ± 5.4	0.998	81.2 ± 5.6	0.995
BSS	124.3 ± 3.7	0.9996	111.9 ± 6.4	0.997
Tears Natural	111.7 ± 4.2	0.9993	102.0 ± 5.1	0.997
Tetracaine *	1790 ± 60 *			
Dextran 7 %	106.7 ± 2.1	0.9998	94.4 ± 6.2	0.996
Dextran 15 %	98.2 ± 1.6	0.9999	84.6 ± 7.0	0.993
Methocel	105.0 ± 18.7	0.984	93.8 ± 8.3	0.992
Celluvisc	141.3 ± 2.1	0.9999	129.6 ± 6.0	0.998
Healon	360 ± 117	0.948	189 ± 94	0.802
Ophthalin	351 ± 42	0.993	184 ± 85	0.825
Oxane	60.3 ± 4.1	0.998	56.9 ± 2.2	0.999
DDS.	---	---	---	---
Silol 5000	28.4 ± 2.1	0.997	30.0 ± 1.3	0.998
PTS	90.2 ± 12.1	0.991	88.0 ± 4.8	0.997

Table 3.4. The Attenuation coefficients and r^2 - values at 193 nm. Observe that Tetracaine (*) was calculated with a different method than the other liquids.

Masking Agents at 213 nm	Att. coeff. μ_t, 3 points	r^2 - value	Att.coeff. μ_t, 4 points	r^2 - value
Perfluorooctane	0.82 ± 0.71	0.719	0.64 ± 0.25	0.863
Perfluorodecaline	11.4 ± 0.6	0.999	10.7 ± 0.4	0.998
NaCl	1.22 ± 0.69	0.858	1.13 ± 0.23	0.960
BSS	5.51 ± 0.45	0.997	5.12 ± 0.34	0.996
Tears Natural	9.45 ± 1.00	0.994	8.96 ± 0.47	0.997
Tetracaine	335.8 ± 27.4	0.997	313.7 ± 14.3	0.998
Dextran 7 %	4.50 ± 0.77	0.985	3.93 ± 0.38	0.991
Dextran 15 %	2.58 ± 0.71	0.963	2.09 ± 0.34	0.974
Methocel	6.12 ± 1.93	0.951	7.02 ± 0.91	0.984
Celluvisc	10.2 ± 1.7	0.985	10.6 ± 0.6	0.996
Healon	34.4 ± 5.0	0.989	36.7 ± 6.0	0.974
Ophthalin	32.1 ± 5.2	0.987	33.8 ± 2.5	0.995
Oxane	19.6 ± 1.7	0.996	18.8 ± 0.9	0.998
DDS	---	---	---	---
Silol 5000	5.73 ± 1.12	0.981	6.11 ± 0.58	0.991
PTS	9.56 ± 3.85	0.922	9.09 ± 1.27	0.981

Table 3.5. The Attenuation coefficients and r^2 - values at 213 nm

Liquids	Refractive index, n for λ=589.3 nm	Abbe number, v.
Perfluorooctane *	1.27	45.0
Perfluorodecaline	1.3122	44.6
Distilled water	1.3327	42.3
NaCl	1.3340	43.0
BSS	1.3346	42.4
Tears Natural	1.3352	42.1
Tetracaine	1.3363	42.0
Dextran 7 %	1.3450	42.3
Dextran 15 %	1.3563	42.0
Methocel	1.3370	42.0
Celluvisc	1.3370	42.0
Healon	1.3357	42.1
Ophthalin	1.3357	42.0
Oxane	1.4040	41.4
DDS	1.4950	37.6
Silol 5000	1.4038	41.8
PTS	1.3816	42.4

Table 3.6. Refractive index and Abbe number for all sample material. Perfluorooctane (*) was outside the scale of the instrument, therefore the refraction index is estimated.

For many of the liquids, the absorbance was observed to increase with the time during the measurement. Especially for Healon, Ophthalin, Oxane and the liquids containing silicon, the increase was significant. To avoid measurement errors, all liquids were measured directly after they were placed in the cell holder in the spectrophotometer.

3.4.2 Direct and Diffuse Absorbance

The diffuse and direct absorbance, corresponding to absorption and attenuation respectively, as a function of the wavelength is shown in Fig. 3.12-13 The measurements were made with the Shimadzu-spectrophotometer and the integrating sphere, described in Ch. 3.2.3. For most of the masking agents, the attenuation is strongly increasing towards shorter wavelengths. Exceptions

are Tetracaine, which has a very high attenuation peak already around 320 nm and DDS, which starts to attenuate already around 280 nm.

3.4.3 Angular Dependence

The measurements made with the fibre cable system, described in Ch 3.2.4, showed no detectable scattering. Every liquid showed an angle dependence similar to the one shown in Fig. 3.11, where the empty QS-cell was placed in a 193 nm light beam.

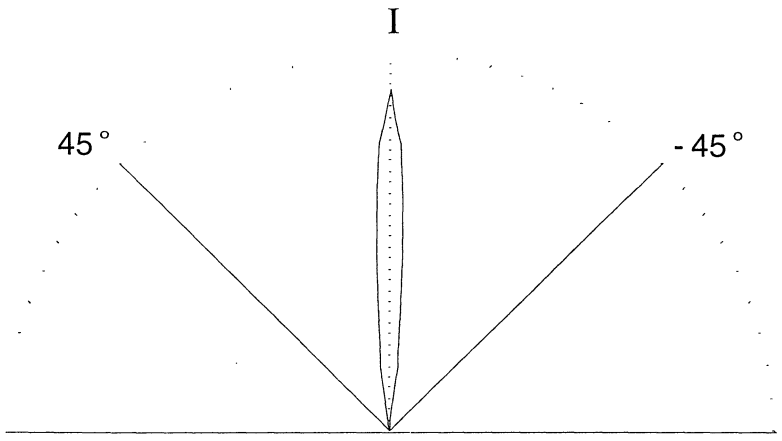

Fig. 3.11 The angle dependence of 193 nm light through an empty QS cell. The from the cell outcoming light intensities, was measured in angles between ± 45°, with the fibre cable system described in Ch 3.2.4. The intensities were plotted in a polar plot and 180°from this plot is shown in the figure.

The transmitted intensity measured outside an 13° - angle against the normal of the cell, never exceeded the noise level of the system.

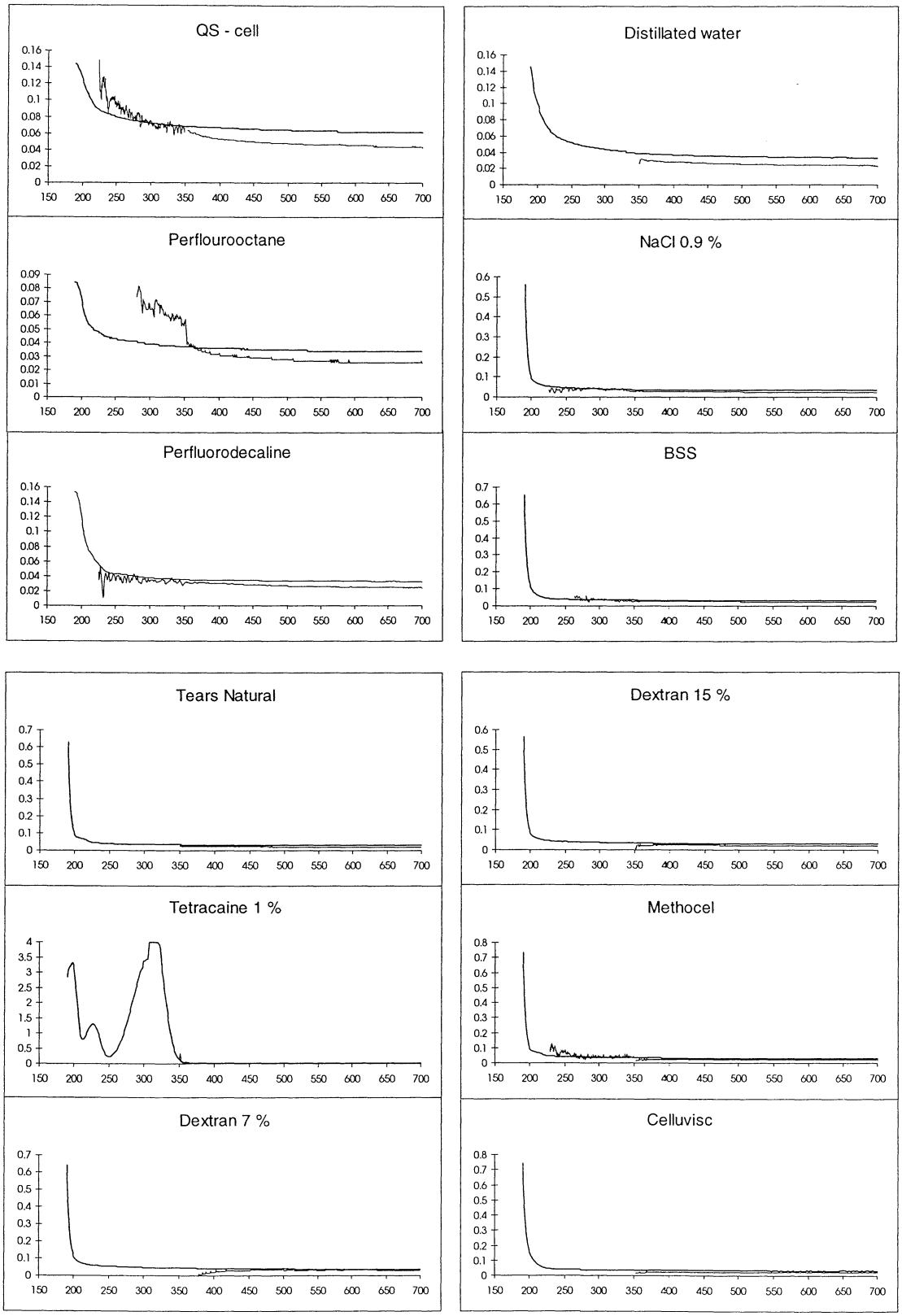

Fig. 3.12 The different liquids measured with a 0.005 cm cell direct in the spectrophotometer and diffuse with the integrating sphere (thin line). The y-axis is absorbance and the x-axis wavelength.

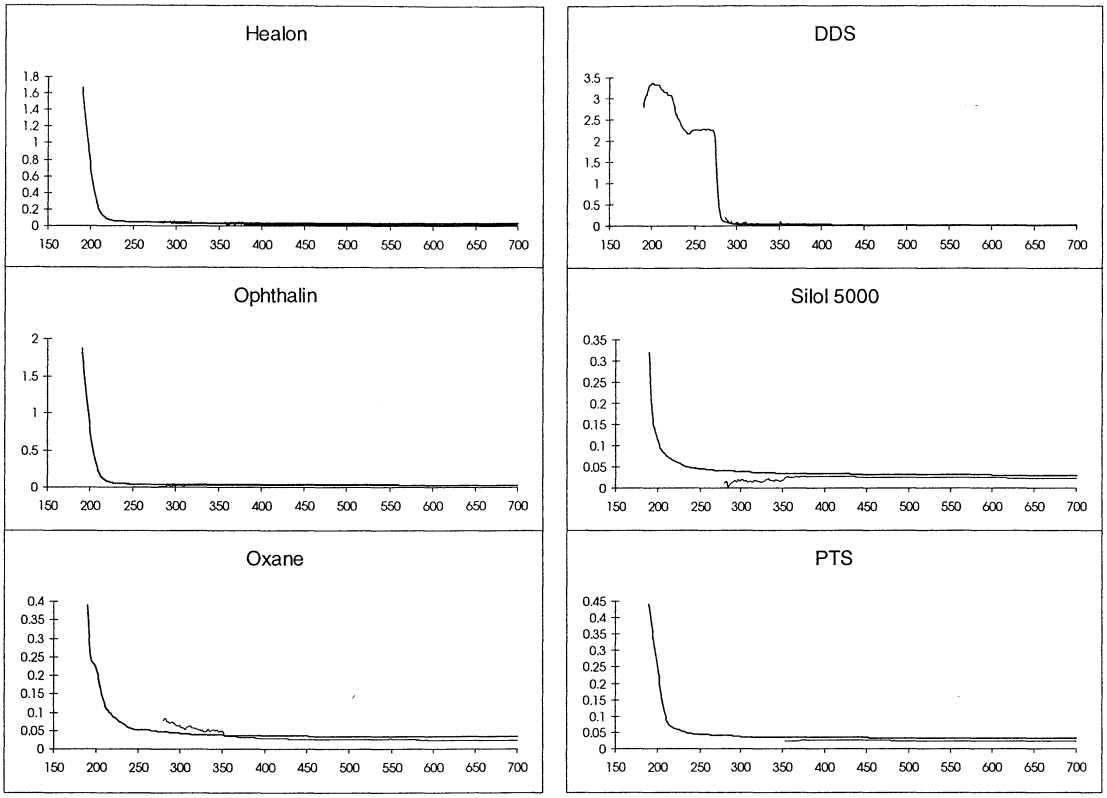

Fig. 3.13: The different liquids measured with a 0.005 cm cell direct in the spectrophotometer and diffuse with the integrating sphere (thin line). The y-axis is absorbance and the x-axis wavelength

3.5 DISCUSSION

3.5.1 Attenuation Coefficient

For all of the masking agents, except Silol 5000, the attenuation coefficients determined at 193 nm are larger when three instead of four pathlengths are used. Furthermore, for many materials the r^2 - values is larger, i.e. the linearity is higher, with three instead of four used path lengths. This is obvious for i.e. Healon Fig. 3.9. Hence, the measurements follow Lambert-Beer - law better when just the three shortest and not all four cells are used.

The reason can be instrumental and/or arise from the sample. If it is instrumental, a likely reason is the stray-light. In the region near vacuum-UV light, the relative stray-light increase, depending on e.g. the attenuation spectra of the liquids as discussed in Ch. 2.1. The, for the investigated masking agents, typical appearance of the absorbance to wavelength curve, with a strong increasing attenuation around 200 nm, makes the relative stray-light percent higher. In Fig. 3.14, spectra measured in the Perkin-Elmer spectrophotometer, is plotted for three samples; for a 0.02 cm and a 1 cm QS - cell filled with the 0.9 % NaCl-solution and for an empty cell of normal glass. Figure 3.15 shows the same for the Shimadzu spectrophotometer, but here the NaCl solution was put into a 0.005 cm QS- cell instead of one with 0.02 cm pathlength. The arrow in Fig. 3.14 shows, what most likely is an large influence from straylight at short wavelengths. The

measured attenuation coefficient for the NaCl - solution was c.a. 90 cm^{-1} at 193 nm. If the solution follow Lambert-Beer law, this would give an absorbance for a 1 cm cell of around 90. However, the measured absorbance is not more than around 2 for the Perkin Elmer and around 2.4 for the Shimadzu. Due to the sensitivity of the detectors, the maximum absorbance possible to measure is 3.5 and 4 for the Perkin-Elmer and the Shimadzu respectively. If the solution is assumed to obey Lambert- Beer law, the straylight percent must therefore be around 10^{-2} and $10^{-2.4}$ respectively, i.e. around 1 %.

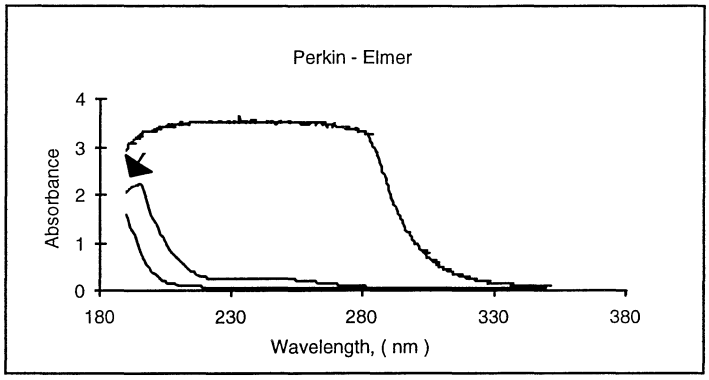

Figure 3.14. Thick lines are NaCl solutions and the thin line is a empty cell of normal glass. The lower NaCl solution were filled in a 0.02 cm QS cell and the upper in a 1 cm - cell.

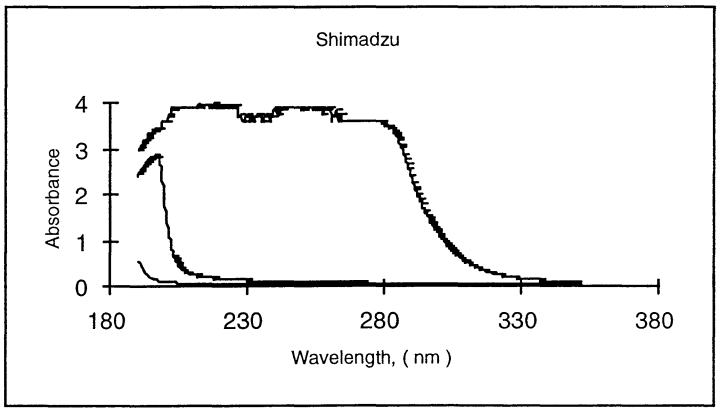

Figure 3.15. Thick lines are NaCl solutions and the thin line is a empty cell of normal glass. The lower NaCl solution were filled in a 0.005 cm QS cell and the upper in a 1 cm - cell.

If the Eq. (3.13) from Ch. 3.2.1 is used, the true absorbance can be estimated.

$$A' = -\log_{10}[\,10^{-A}\,(1-s) + s\,] \qquad (3.13)$$

If stray-light, s, is 1 %, apparent absorbance depend on true absorbance like Fig. 3.16. The plot shows the strong influence of stray-light when high absorbance is measured. Further is the higher absorbance for normal glass at 193 nm, than for the NaCl - solutions (in Figures 3.14-15), most likely a result of the attenuation of the stray-light by normal glass up to 300 nm, which

gives less apparent stray-light. Our measured absorbance spectra look, however, mostly like the ones for the NaCl- solution. As a consequence, the straylight at 193 nm should be around 1 % for most of the liquids. The stray-light may therefore explain a large portion of the non-linearity seen in Figures 3.9-10 for most of the liquids at 193 nm.

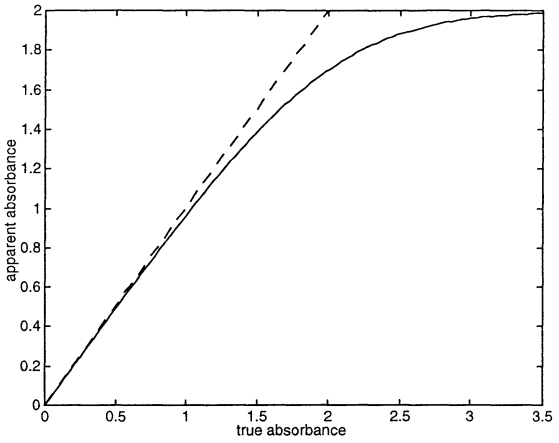

Fig.3.16. Apparent absorbance vs. true absorbance

As mentioned above, the masking agent itself could as well be the reason for the unlinearity. Intermolecular effects caused by interactions between the different particles in concentrated solutions[30] could give rise to a deviation from Lambert Beer-law. However, this effect should then appear for all pathlengths and not just for the long ones. However, some of the masking agents e.g. the NaCl solution, Oxane and Healon, especially at 193 nm, show a bent graph form, see Fig 3.9, what indicates intermolecular effects.

Another important factor is the scattering caused by the masking agents. Scattering does not influence how well Lambert Beer-law is obeyed, but makes the absorption coefficient seem higher than it is, see Ch. 3.1, Eq. (3.6) and (3.7). No scattering could be measured in the experiments, though there could be some according to Ch. 3.1.2.

The spectral band width may influence the results more than previously expected in Ch 3.3.1. In Fig. 3.17 the influence from the Spectral Band Width (SBW) is shown at 193 and 213 nm for the BSS and the NaCl 0.9 % - solution. The solutions were measured in cells of different pathlengths to check the dependence of SBW at different absorption levels. The diagrams show a distinct influence for high absorbance. The reason is the strongly increasing absorbance for the BSS and the NaCl 0.9 % solution towards shorter wavelengths. With a to broad SBW, the spectrophotometer can not reproduce a true spectrum. It will be slightly smoothed out. To check the influence on the results, Tears Natural and Celluvisc were measured also with 1nm SBW, besides the normally used SBW of 2 nm. No change of the absorption coefficient could be observed at 213 nm, whereas at 193 nm, the absorption coefficient increased from 141.3 to 149.1 cm^{-1} for Celluvisc and from 111.7 to 115.3 cm^{-1} for Tears Natural.

[30] Sommer L., Analytical Absorption Spectrophotometry in the visible and the UV - The Principles, (Studies in Analytical Chemistry) , Elsevier, Amsterdam, p.24, 1989.

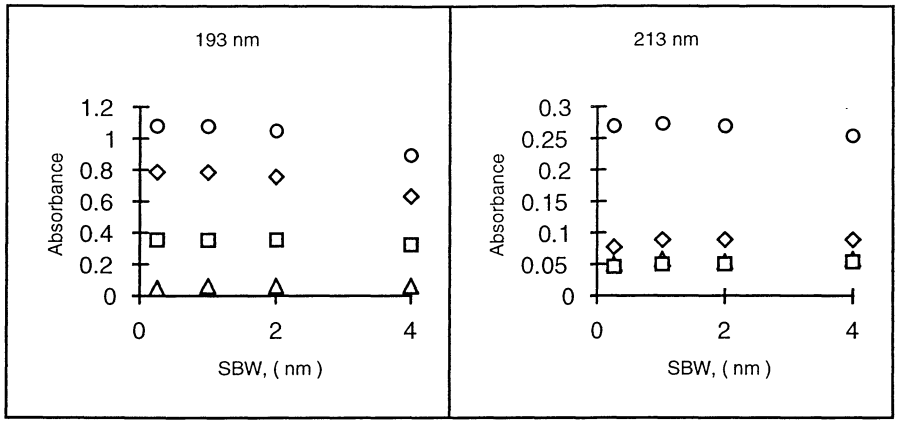

Fig. 3.17 The absorbance dependence on the SBW. Circles are BSS in a 0.02 cm cell, angled squares are the NaCl 0.9 % - solution in a 0.02 cm cell, normal squares are BSS in a 0.005 cm cell and triangles are NaCl 0.9 % solution measured with a 0.001 cm cell.

Besides unlinearity, some of the graphs in Figures 3.9-3.10 have large deviations from the straight line at every pathlength. At 213 nm, the reason can be that the absorption is often very small. Small absorbances give rise to large repeatability errors, see Ch. 3.2.1. Another reason can be the washing of cells. Although the cells were carefully washed, the transmission of the QS - cells varied ± 5 %. This could imply a significant influence on the result for small absorption. For e.g. the data for Perfluorooctane and the NaCl-solution, shown in Fig. 3.9, this could be the reason. For viscous materials like Healon and Ophthalin, the deviations can be connected to the filling of the cells. With viscous materials it appeared difficult to fill the cell in exactly the same way from measurement to measurement, giving rise to fluctuations in pathlength (part of the liquid flowing between the two parts of the cell) and as a consequence in the absorbance.

The observed variation of the absorbance with time, could be caused by temperature fluctuations. The temperature in the Lambda-6 spectrophotometer was observed to be between 25-30 °C, whereas the room temperature stayed around 21 -22 °C. Another, for the following ablation experiments more important reason, could be the UV light. For some material e.g. PMMA[31], the absorption coefficient increases, within seconds, due to UV - light. The UV - light may cause chemical changes in the material, which may give rise to the increase.

3.5.2 Direct and Diffuse Absorbance Spectra

For most of the liquids, the direct and diffuse absorbance measured as a function of the wavelength (Fig. 3.12-13) has a strong increasing attenuation around 200 nm. Exceptions are Tetracaine, which has a very high attenuation peak already around 320 nm and DDS, which starts to absorb already around 280 nm.

The diffuse spectra measured with an 0.005 cm QS - cell in the sample holder shows an unexpected difference between direct and diffuse absorption. The difference appear, however, also for the empty QS - cell why nothing can be concluded from this deviation. Below 350 nm, the integrating sphere starts to act unreliable, due to the low signal to noise ratio and the results can not be trusted.

[31] Kueper S., Ablation mit UV-Laserlicht (Dissertation), Goettingen, 20-46

To get a lower signal to noise relation, either the light source could be changed to a stronger one or / and the coating of the integrating sphere could be replaced with a more reflective one. A stronger light source is e.g. a Xenon lamp[32] and a better coating is e.g. $MgSO_4$ [33]

3.5.3 Angular Dependence

The measurements with the fibre-optic-system showed no intensity higher than the noise level outside an 13°- angle against the pathway of the beam. Hence, the scattering could be as large as the noise level for all angles between 13° and 90°. The integrated intensity of this scattering would correspond to the attenuation for each masking agent. Hence, nothing can be told about the scattering from the measurements with this system. On the other hand, with other materials and at higher wavelengths, scattering was proved with this system (not shown). Therefore, with a stronger light source, the system would be useful also for wavelengths around 200 nm.

[32] Svehla. G, Comprehensive Analytical Chemistry, **4,** Elsevier, Amsterdam, p.139, 1975
[33] Svehla. G, 284-285

4. Laser Ablation

4.1 Introduction

The photons from the laser excites the molecule to a higher electronic, vibrational or rotational state. Therefore, the absorption of laser light may lead to photochemical, photothermal and photomechanical interactions with the target material.[34] An example of photochemical interaction is a covalent bond breaking. If the photon energy is high enough to excite the electron to an electronic state which is not bound, the molecule dissociate. Then it will form radicals or break. Photothermal interactions are e.g. interactions which convert the laser energy into heat and diffuse the heat within the material. Photomechanical effects may be thermoelastic expansion caused by the heating of the material and recoil caused by the ejection of ablated material. [35]

Both photothermal effects and bond breaking produces a crater by ejection of material. However, an undesired effect of laser ablation is thermal damage to material adjacent to the crater. As a result of the absorption of laser energy, the temperature rise and the heat is conducted into material e.g. tissue surrounding the crater. This is the most important side effect to be concerned for a successful ablation of a material. To minimise this effect, it is advantageous to use a pulsed laser instead of a continuos wave (cw) - laser for ablation. First, if the laser pulse is shorter than the thermal relaxation time of the tissue, the zone of damage may be reduced. Second, if sufficient energy is delivered, the tissue is removed before heat has been transferred to surrounding material.[36]

The last finding (sufficient energy) may be possible to apply to PMMA as well. PMMA (Polymethylmethacrylate) is a plastic which will be used in the experiments. The quality of the ablated surface of PMMA is found to be better for ablation at 193 nm (= higher energy) than at 248 nm and obvious traces from thermal processes are found at 248 nm.[37]

Another phenomenon that may influence the ablation is the mechanical properties. Walsh et.al [38] has described the effect of mechanical properties for pulsed CO_2 - laser ablation and concluded that "mechanical strength of tissue can effect mass removal by pulsed laser ablation by as much as a factor seven".

The formation of bubbles that has been reported during irradiation of different materials, e.g. 193 nm excimer laser ablation of NaCl solutions of different concentrations[39], may as well have an influence on the ablation process.

---

[34] Kueper S. Ablation mit UV-Laserlicht (Dissertation), Goettingen, p.5, 1989

[35] van Leeuwen TG, et al., Pulsed Laser Ablation of Soft Tissue *Optical Thermal Response of Laser Irradiated Tissue,* Plenum Press, New York, 709-711, 1995

[36] van Leeuwen TG et al, 715-716

[37] Kueper S. Ablation mit UV-Laserlicht (Dissertation), Goettingen, p.12, 1989

[38] Walsh JT Jr., Pulsed CO_2 Laser ablation of tissue, effect of mechanical properties, *IEEE Trans. Biomed. Eng.,* **36**, 1195-1201, 1990

[39] Turovets L et. al., ArF Excimer laser induced bubble formation during irradiation of NaCl solutions, *Photochemistry & Photobiology.* **60** No. 5, 1994

T. F. Deutsch[40] states for IR - laser that: "In a clinical situation in which ablation occurs with a fluid, such as blood, surrounding the target, the mechanical effects may be enhanced because of the confinement of the water vapour formed". T.G. van Leeuwen et. al.[41] states for tissue ablated by excimer laser pulses: "In air, the water vapour will easily expand and therefore craters without adjacent tissue damage are formed. If the expansion is hindered by a contact catheter, it may expand within the tissue. Then the ablation process is more violent". These findings indicates, that when tissue is any way constrained, the laser ablation process may be enhanced.

This description of the laser ablation process does not in any way try to be complete, but tries to describe a few, for the following experiments, important parts. Moreover, the above findings show that the ablation is not fixed through the attenuation coefficient, but depends also on other properties of the target, such as its reflectivity, density, specific heat, latent heat, temperature of melting and of the laser beam, such as repetition rate, energy per pulse and pulse length.[42]

4.2 Instruments and Materials

An 193 nm excimer laser was used to ablate material, a profilometer as measuring system and PMMA - discs were used as base material with different irregular patterns that were filled with the previous specified masking agents (Ch. 2).

4.2.1 The Excimer Laser

Excimer lasers are trigged by a fast electrical discharge in a mixture of F_2 and HCl and halogens. The electrical discharge raises the energy level of the rare gas atoms, so that they react with the halogen molecules to form compounds, so called **exc**ited **dimers** (excimers), such as ArF. While returning to the ground energy level, these compounds dissociate and fluoresce strongly in the ultraviolet spectral region. When the gas is contained in a resonator, the laser effect with coherent light is produced.[43, 44]

The laser used is an ArF 193 nm pulsed excimer laser model Keracor 116 (Technolas). This laser has been designed for both Photo Therapeutic Keratectomy (PTK) and Photo Refractive Keratectomy (PRK). The optical design is displayed in Fig. 4.1

---

[40] Deutsch, TF, IR-Laser Ablation in Medicine: Mechanism & Applications,*Lecture Notes in Physics,* **389**, Springer Verlag, Berlin-Heidelberg, p.111, 1991

[41] van Leeuwen TG et. al., p. 742

[42] van Leeuwen TG et al., p. 716

[43] Svanberg S. p.208

[44] Technolas GMBH, Keracor 116, Excimer laser for corneal surgery, (Instruction paper)

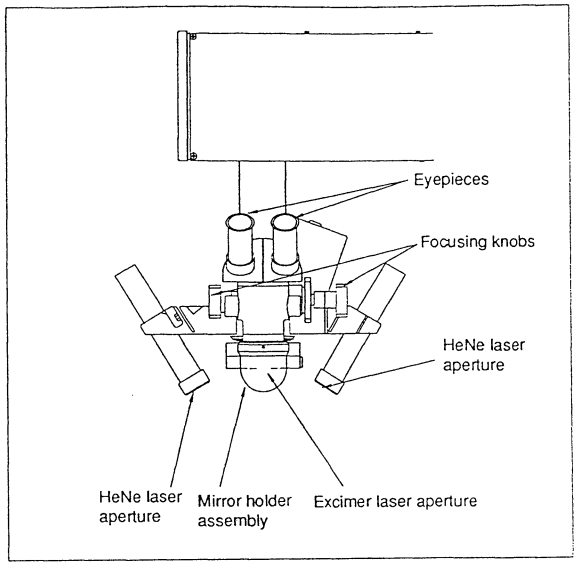

Fig. 4.1 The excimer laser with the two HeNe-lasers used to positionize the target, the excimer laser beam delivery system and the operating microscope.(From Ref. 44)

Two HeNe - lasers are used to positionize the target on the right location. The Keracor 116 uses an Iris diaphragm to vary the beam diameter within xx and yy mm. The maximum repetition rate is 30 Hz and the fluence per pulse is adjustable between 120 and 200 mJ / cm^2 .

4.2.2 The UBM Microfocus Measuring System

The UBM Microfocus measuring system is a profilometer. It determines the profile of a surface in two or three dimensions. The instruments works on the principle of a laser beam kept focused at the surface during the scanning over the surface. From the adjustments of the focusing optic, the profile can be calculated. The beam from a diode laser at 780 nm strikes the surface and the reflected radiation is received in a differential photodiode. The properties of the reflection makes it possible to calculate the adjustments of the focusing optic.

4.2.3 The PMMA - discs

Polymethylmethacrylate (PMMA) is an organic material (plastic), which shows excellent results when ablated with an 193 nm ArF excimer laser. In previous works, the ablated surface was found smooth and only small damage to the material, adjacent to the crater, was observed[45]

The PMMA used is a medical grade one, enhanced with UV-absorber (PMMA-CQ-UV1, ICI England), This material is currently used for manufacturing of intraocular lenses and keratoprotheses.

Because it is an organic material, like the cornea, the model for the ablation experiments was produced in PMMA. Two patterns were milled into the PMMA discs with a model FP 3CC Deckel precision mill, one with slots and cubes (Fig 4.2) and one with holes (Fig. 4.3). The whole PMMA - disc with the cube pattern can be seen in Fig 4.4. The pattern on the surface of the discs were intended to be a model of the irregularities that can arise on the cornea. However, above all, the patterns were designed to make measuring of the ablation of the masking agents possible.

[45] Kueper S. p. 2

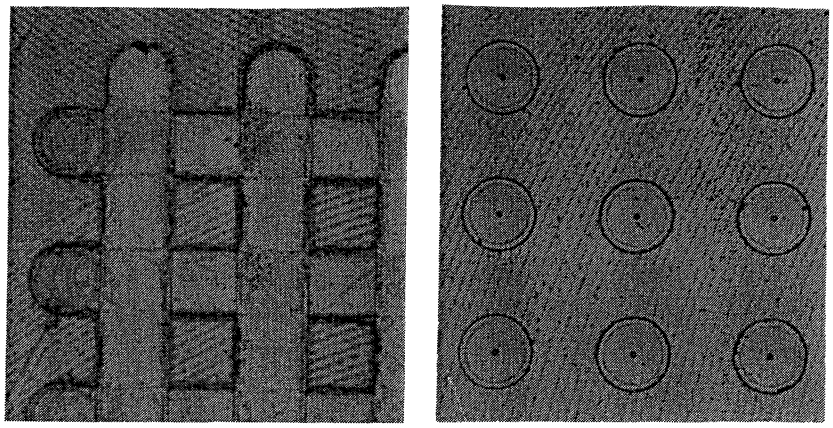

Fig 4.2-3 The cube and the hole patterns. The photos are recorded with a model Dialux 22 (Leitz) microscope in bright field, with the 2.5x objective. This microscope had an integrated camera model Wild MPS 52. The pattern on the photos are shown in a 2x enlargement.

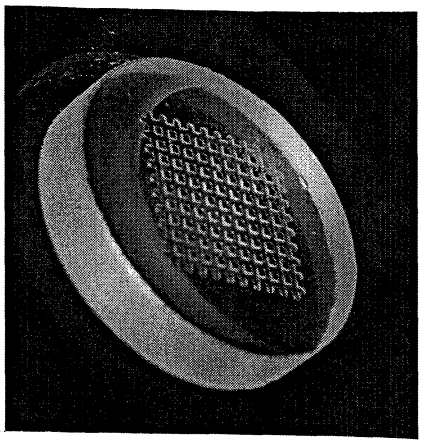

Fig 4.4 The PMMA - disc with the cube pattern, recorded in a 50°angle, with a Nicon camera in a reflection microscope with an 6.0x objective. The PMMA disc is shown in a 2x enlargement.

The depth was for both patterns aimed at 40 μm, similar to the highest ablation depth used in PRK/PTK. The holes had a 0.5 mm diameter and a 1 mm distance row to row (hole centre to hole centre), in both directions. The cube pattern resulted in cubes with a surface area of 0.5 x 0.5 mm^2 and the slots had a diameter of 0.5 mm.

4.3 Method

4.3.1 Choice of Method

When the ablation of a liquid has to be quantified, a problem arise. A liquid does not form an ablated crater that can be measured, like a solid. A liquid looks approximately the same before and after an ablation (naturally depending on the viscosity of the liquid, which is ablated). In spite of that, the ablation could be measured through e.g. weighing the liquid before and after the

ablation and calculate the difference. The volume before and after ablation could also be used as variable.

However, the for these experiments chosen method is to use PMMA discs with different patterns. The previous specified masking agents are applied to the discs and after the laser ablation, the change of the patterns can be observed and hopefully quantified.

One large advantage of this method, is that the PMMA disc can be seen as a model of a human cornea and the pattern as a model of irregularities on it. Though, one has to keep in mind that PMMA and not cornea is used as base material.

4.3.2 Application

The masking agents were applied in two ways: either the liquid was put on the disc and the redundant liquid was removed with a microsurgical sponge without further manipulation, or it was levelled out over the pattern with a microsurgical sponge and the side of a sterile needle. The quality of the application was controlled in the microscope of the excimer laser before the ablation.

Manipulated	Dextran 7%, Dextran 15%, Methocel, Celluvisc, Healon, Ophthalin and Oxane
Not manipulated	Perfluorooctane, Perfluorodecaline, Distilled water, NaCl 0.9 %, BSS, Tears Natural, Tetracaine

Table 4.1. How the liquids were applied

4.3.3 Ablation and Measurement

To make better use of the pattern, each PMMA model was ablated twice. The models were ablated once in one corner of the pattern and then in the opposite corner once more. Each time with a different liquid and with 320 pulses. 320 pulses is equal to a ablation depth of around 80 micrometer in the cornea if it does not move during the operation. The beam diameter was 5 mm and the repetition rate 20 Hz. No more liquid was applied during the ablation process. The models were washed with optical ethanol and distillated water before and between the ablations.

To quantify the ablation, the previously described UBM instrument was used. The profiles of the ablated PMMA models were recorded by scanning along a diagonal line, across the samples, see Fig. 4.5.

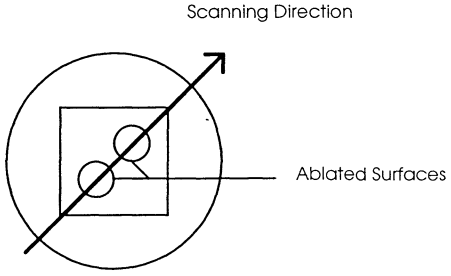

Fig. 4.5. How the scanning with the UBM instrument was made, straight across the PMMA - disc.

The instrument was carefully centred over the patterns. It had to be positionized right over the holes or cubes of the patterns and the scanning direction had to be exactly 45° across the patterns. Otherwise the profiles of the discs would not be correctly reproduced and all the cubes and holes would not have been measured to the same size, see fig. 4.6 a. Two line scans were made on each model. The second time, one row besides the first, see fig 4.6 b.

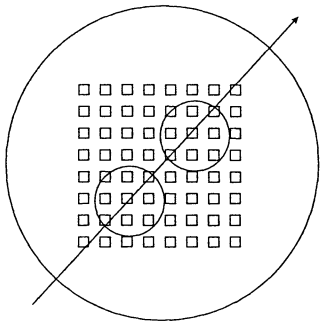

Figure 4.6 a)
The scanning direction is not right over the pattern, giving rise to a profile with different sizes on the cubes

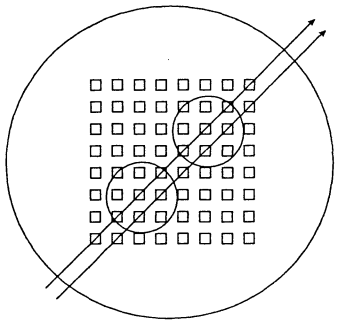

4.6 b)
The two profile scans .

The unablated PMMA - models, i.e. the PMMA - models with a milled pattern but before the laser ablation, were not perfectly even. As a consequence, the ablated models were also warped, as shown in Fig. 4.7 a. Therefore the produced profile curves were artificial straightened with a linear algorithm, Fig. 4.7 b. The program used for the straightening belonged to the software of the UBM - instrument.

With the same program, the straightened profiles were measured. Each top and bottom part was integrated and an average was calculated. In Fig. 4.7 an example of an integrated top and an integrated bottom part is surrounded with rectangles.

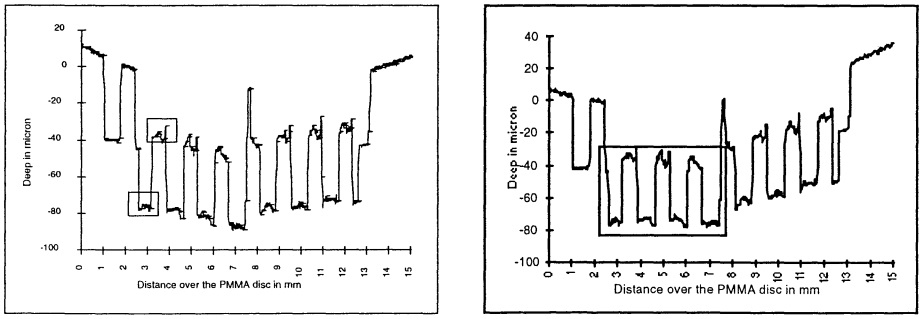

a) *b)*

Fig. 4.7 An example of a scanned profile before, a), and after, b), fitting with the UBM-program.

In the ablated region, surrounded in Fig. 4.7b the first measurable part, indifferent if top or bottom part, was subtracted from the closest following part. To each scanning profile 2-4 such differences could be calculated, which made complete 5 - 7 calculated differences for the two

profiles belonging to each masking agent. For these 5 - 7 values an average and a 95 % confidence interval was calculated. The same measurements and calculations were made for the unablated region. However, for the unablated region, just 4-5 difference values could be calculated, due to how the profile was scanned..

For each masking agent, the average difference of the ablated region was now subtracted from the average difference of the unablated region. Moreover the average differences before and after ablation, μ_{before} and μ_{after}, were tested against the hypothesis that $\mu_{before} = \mu_{after}$. The higher the level of significance (in percent), the higher is the probability that the distance from top to bottom has not changed due to the ablation.

The significance test as well as the determination of confidence interval, assume the populations to have normal distribution. Moreover, the significance test assume the variance to be the same for the "Before" and the "After" populations. To check this, more values are required then were produced in these experiments.

4.4 Results

The application of the masking agents on the discs was problematic. The liquids tended to form drops and not to spread over the surface. Above all Dextran 7 % and Dextran 15 % were difficult to apply to the PMMA - discs. It was also difficult, with the microscope belonging to the excimer laser, to tell how well applied the masking agents were.

All masking agents displayed fine bubbles during the ablation. Oxane and the two Dextran solutions produced most bubbles, like foam. Healon, Ophthalin, Methocel and Celluvisc had intermediate bubble formation and the other liquids low bubble formation.

One of the straightened profiles for each masking agent and each pattern, except those containing silicon, are presented in Figs. 4.9 - 4.10. Liquids containing silicon were told to, due to ablated particles, be able to damage the instrument. Therefore, no liquid containing silicon was tested. Fig. 4.9 contains the profiles from the square patterns and Fig. 4.10 those from the hole patterns. When the x-axis in the profile curves is marked from one and upwards, the profiles originate from the first scanned part, down to the left in Fig. 4.8. When the x-axis is marked from 7 or 8 and upwards, the profile originates from the second ablated part, up to the right in Fig. 4.8.

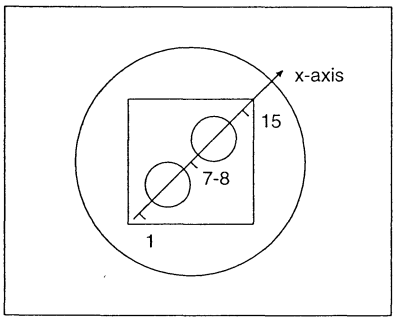

Figure 4.8 Numbering of the x-axis.

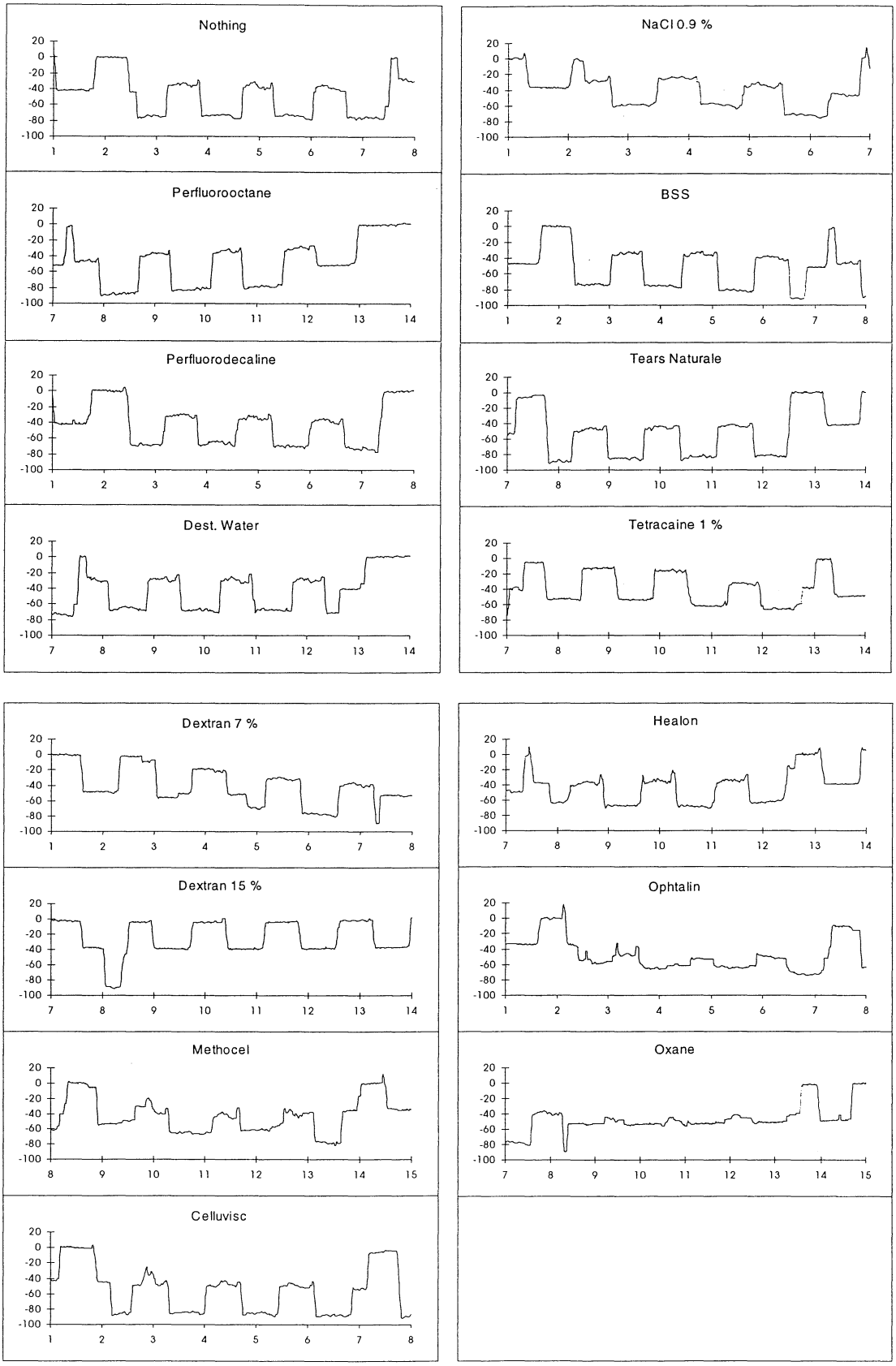

Fig 4.9. The profile of the ablated cube pattern. x-axis in mm and y-axis in μm.

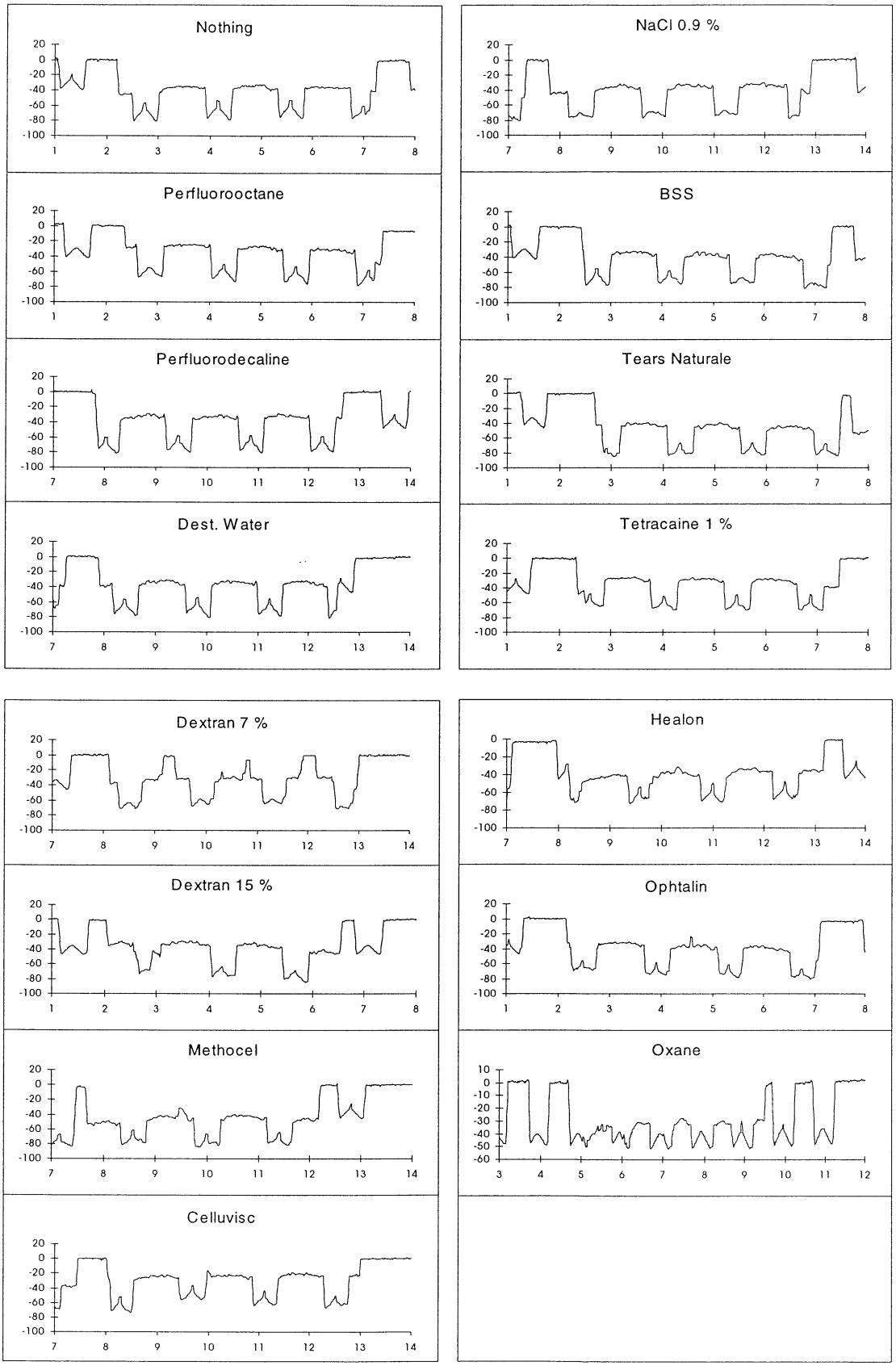

Fig 4.10. The profiles of the ablated hole pattern. x-axis in mm and y-axis in μm.

The conical form of the bottoms of the hole patterns, Fig. 4.10, is due to the manufacturing of the patterns in the mill.

In Tables 4.2 and 4.3. below, the statistical results are listed. The second column contains the average differences between tops and bottoms before ablation, calculated as described in the previous method section. The third column contains the average differences after ablation. In the fourth column the difference between before and after ablation is listed. The significance column, finally, contains the level of significance in percent for the zero-hypothesis, i.e. the hypothesis that the masking agent has **not** influenced the ablation result. This is done under the assumption that for a PMMA- disc not covered with any liquid, the tops and bottoms will be equal ablated, i.e. the profile for the ablated part of the disc will be a copy of the original one but at a lower level. The higher the significance percent, the higher is the probability that the masking agent has not influenced the ablation result. When no significance level is present in the table, the hypothesis was rejected at the 0.1 % level, which means that the possibility is large that the masking agent has some influence on the ablation process.

The profiles of the ablated surfaces are always, rougher than the unablated surface. In general, the profile curves tend to get rougher, the larger the values in the "difference"- columns in tables 4.2 and 4.3 are. Oxane is here an exception.

Liquid	Before	After	Difference	Significance
Nothing	42.1 ± 0.6	40.0 ± 1.1	2.0	0.1 %
Perfluorooctane	48.4 ± 2.9	49.0 ± 1.8	- 0.6	> 5 %
Perfluorodecaline	41.0 ± 2.8	35.0 ± 3.3	6.0	0.1 %
Dist. Water	42.1 ± 0.6	37.8 ± 1.4	4.3	
NaCl 0.9 %	37.9 ± 1.8	31.9 ± 5.3	6.0	1 %
BSS	48.4 ± 2.9	40.0 ± 1.3	8.4	
Tears Natural	43.1 ± 1.8	39.7 ± 1.1	3.3	0.1 %
Tetracaine	47.7 ± 1.5	35.1 ± 9.5	12.6	0.1 %
Dextran 7 %	48.4 ± 2.9	40.7 ± 5.2	6.6	1 %
Dextran 15 %				
Methocel	34.8 ± 0.7	21.3 ± 4.7	13.4	
Celluvisc	47.7 ± 1.5	35.9 ± 4.2	11.8	
Healon	37.9 ± 1.8	27.3 ± 5.8	10.6	0.1 %
Ophthalin	34.8 ± 0.7	14.6 ± 4.6	20.2	
Oxane	48.4 ± 2.9	6.3 ± 2.2	40.9	

Table 4. 2. The ablation results for the square pattern

Liquid	Before	After	Difference	Significance
Nothing	36.2 ± 4.6	33.4 ± 2.3	2.8	> 5 %
Perfluorooctane	37.0 ± 2.9	37.5 ± 1.2	- 0.5	> 5 %
Perfluorodecaline	37.0 ± 2.9	34.1 ± 1.4	2.9	1 %
Dist. Water	36.2 ± 4.6	34.8 ± 0.9	1.4	> 5 %
NaCl 0.9 %	36.7 ± 2.7	36.0 ± 2.4	0.6	> 5 %
BSS	36.7 ± 2.7	31.5 ± 2.1	5.2	1 %
Tears Natural	37.0 ± 1.1	31.6 ± 3.6	5.5	0.1 %
Tetracaine	40.1 ± 1.9	35.3 ± 2.0	3.1	0.1 %
Dextran 7 %	39.2 ± 1.5	37.8 ± 2.6	1.4	> 5 %
Dextran 15 %	39.2 ± 1.5	37.8 ± 3.3	1.4	> 5 %
Methocel	37.0 ± 1.1	30.8 ± 2.9	6.2	0.1 %
Celluvisc	40.1 ± 1.9	34.3 ± 6.2	5.8	1 %
Healon	36.9 ± 3.3	24.4 ± 1.5	12.5	
Ophthalin	36.9 ± 3.3	33.5 ± 1.5	3.4	0.1 %
Oxane	43.1 ± 1.8	10.7 ± 4.93	32.4	

Table 4.3. The ablation results for the hole pattern.

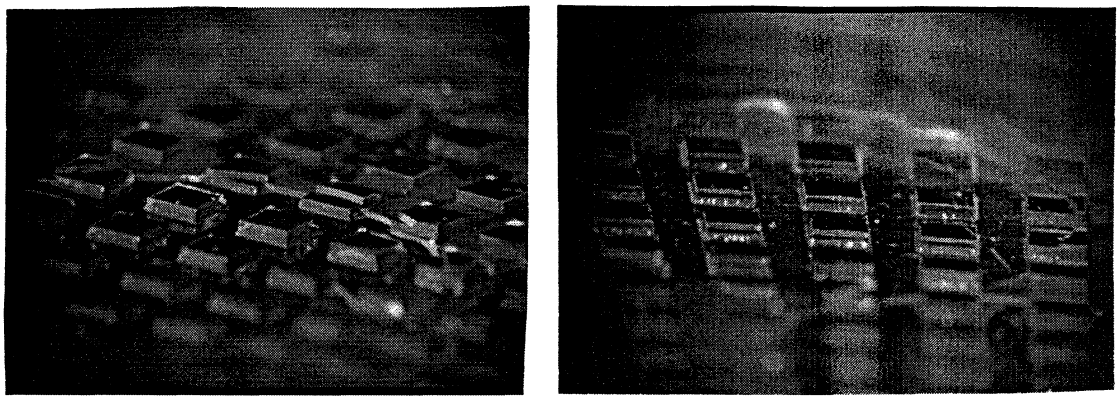

Figure 4.11. Disc with no applied masking agent photographed in angle.

Figure 4.11 shows two photos of a PMMA-discs in c.a. 50° angle against the normal. The disc was ablated without any applied liquid, and the photos were made with a Nikon camera in a reflection-microscope with an 6.0x objective.

Figures 4.12 - 4.20 are photos made with a model Dialux 22 (Leitz) microscope, that had an integrated camera model Wild MPS 52. The photos were made in bright field with an 2.5x objective.

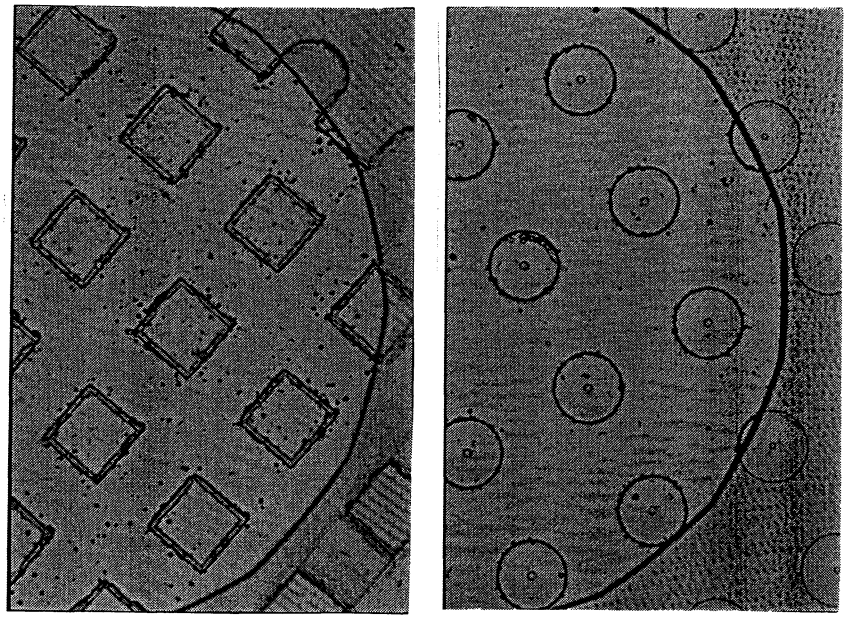

Figure 4.12 a) Cube pattern with no masking agent b) Hole pattern with no masking agent

Picture 4.12 shows the two patterns ablated without masking agent. For both patterns (holes and cubes), Perfluorodecaline, dist. water, NaCl, BSS and Tears Natural, show no significant difference to these two photos, concerning the irregularity grade. For the hole pattern the same is true also for Tetracaine and Celluvisc .

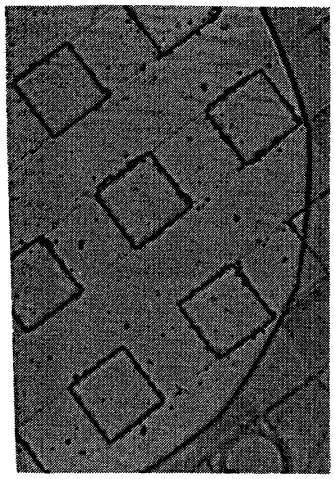

a)

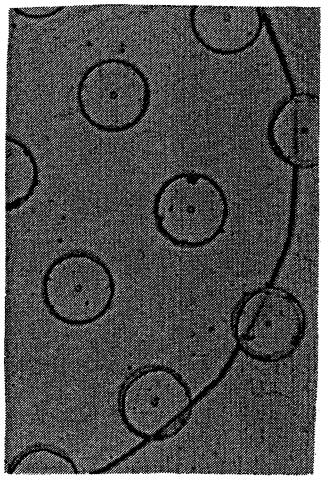

b)

Figure 4.13 a-b. Perfluorooctane

a)

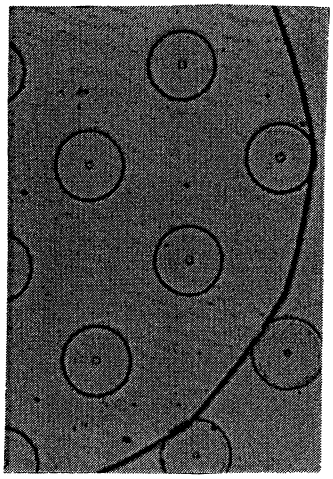

b)

Figure 4.14 a-b. Healon

In Fig. 4.13, ablated patterns filled with Perfluorooctane can be seen. Especially the cube pattern shows less irregularities than the corresponding pattern for no liquid (Fig 4.13 a).

Healon on cube pattern, Fig. 4.14 a show more irregularities than Fig. 4.12 (no liquid). On the other hand, Healon on hole pattern (Fig. 4.14 b), looks as smooth as Fig. 4.12.

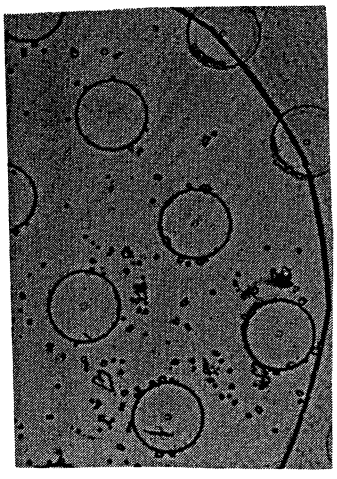

a)

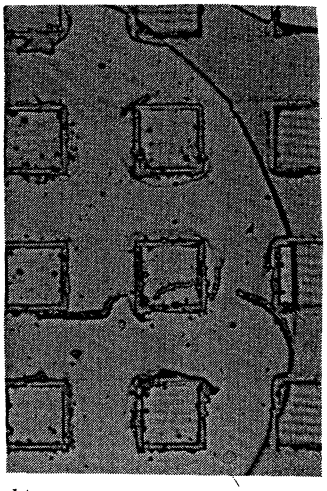

b)

Figure 4.15 a-b. Ophthalin

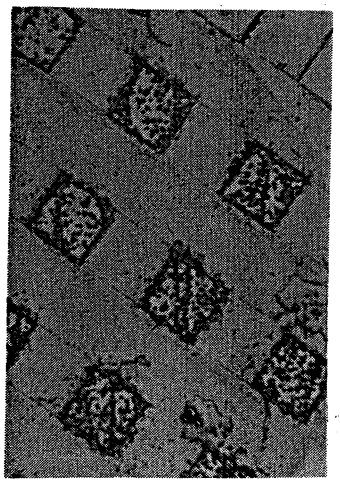

a)

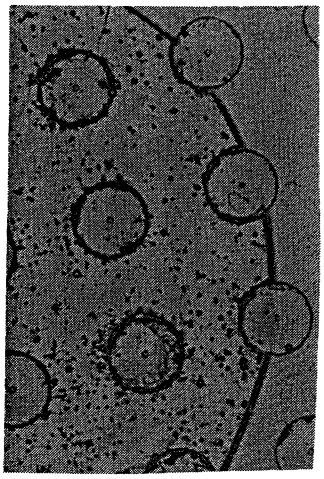

b)

Figure 4.16 a -b. Oxane

Ophthalin on the hole pattern, Fig. 4.15 b, show many small irregularities. Most from these small irregularities, contains, however, the photos of Oxane (Fig 4.16).

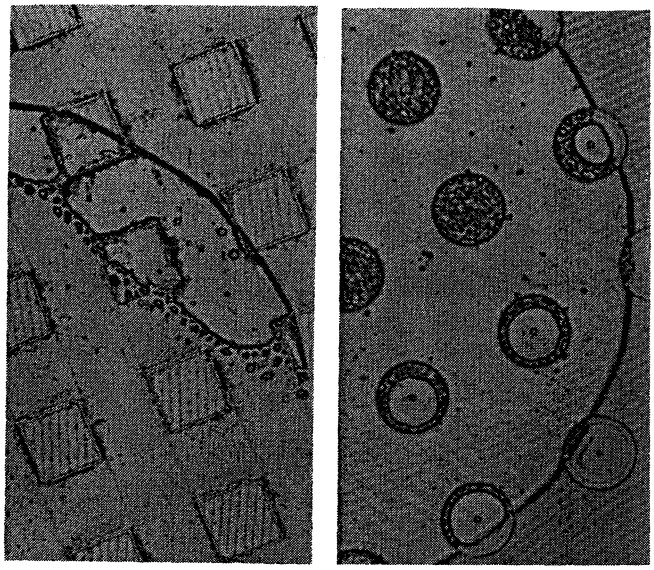

a) b)

Figure 4.17 a-b. Dextran 15 %

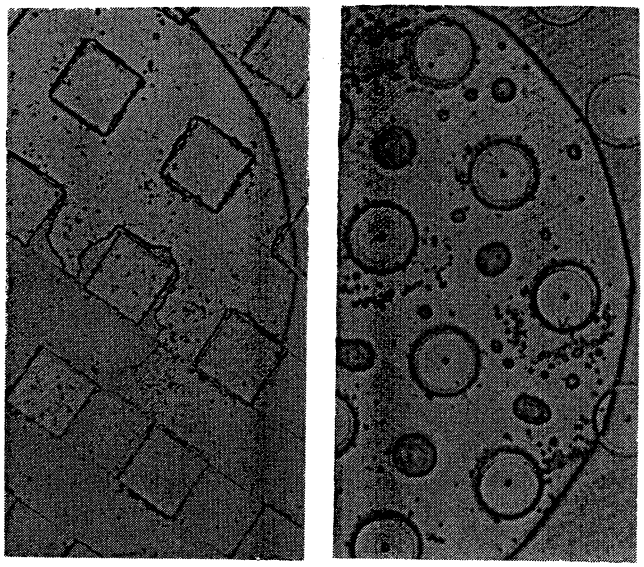

a) b)

Figure 4.18 a-b. Dextran 7 %

Dextran 15 % on a hole pattern (Fig 4.17 b) looks similar to the corresponding picture of Oxane. Figure 4.18 a shows Dextran 7 % on cubes. The photo shows a sharp edge were the bottom surface change from ablated to unablated. This phenomena can also be seen for Dextran 15% (Fig. 4.17 a), Methocel (Fig. 4.19 a) and Tetracaine on the cube pattern.

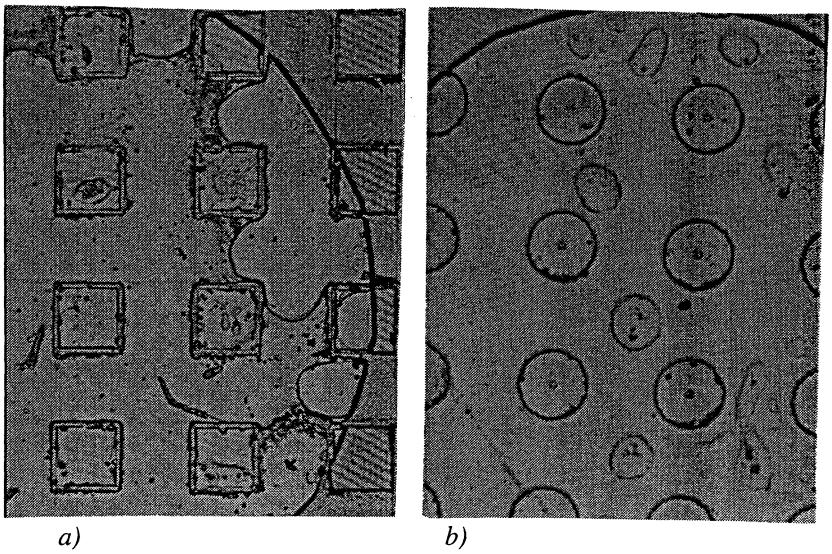

a) b)

Figure 4.19 a-b. Methocel

Finally, Fig. 4.19 a (Methocel on holes) shows an example of conical tops, see the arrow. These can also be found on the hole pattern covered by Dextran 7 %. For the last mentioned liquid the surface in addition is covered with a lot of irregularities, see Fig. 4.18 b.

4.5 Discussion

4.5.1 Application and Ablation

Some profile curves show influence from how the masking agents were applied. Dextran 15 % and 7 % has the property to form drops on the surface of the PMMA disc. These drops can not be levelled satisfying, see Fig 4.21. The shape of the profiles of Dextran 15 % and 7 % in Fig. 4.9 and Dextran 7 % in Fig 4.10 is most likely the results of this problem. The conical peaks seen for Dextran 7 % in Fig. 4.10 and from above in 4.18 b, are probably caused by small drops, preventing the laser beam from reaching the underlying PMMA disc.

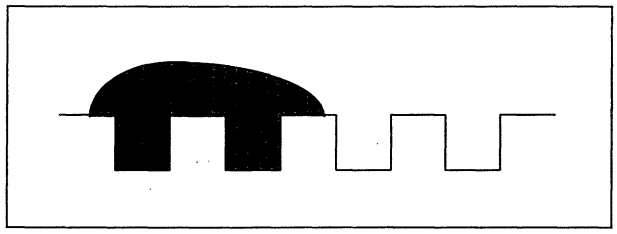

Fig.4.21. The thick layer caused by the drop form stops the light from ablating the surface.

Tetracaine in Fig 4.9 has a profile curve which shows a large, almost unablated part towards the disc centre. The reason may be the shape of the PMMA discs. The discs were, as mentioned, slightly sloping downwards against the centres. For Tetracaine, which is a fluent, almost volatile liquid this shape may have caused the liquid to gather in the centre, see Fig.4.22.

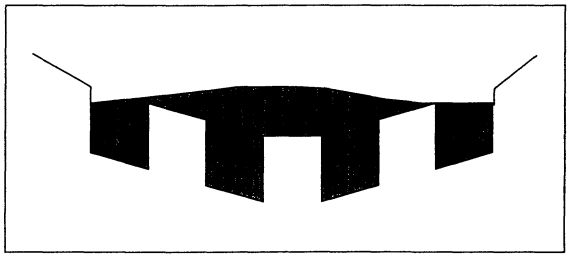

Fig. 4.22. Liquid gathering in the centre of the PMMA-disc.

There are no connections between the holes in the hole pattern. As a consequence the masking agents may sometimes not by themselves spread over the surface. This is a disadvantage for the hole pattern compared to the square pattern. Hence, the liquids may settle irregular, as in Fig.4.23. The Celluvisc profile in Fig. 4.10 is probably a confirmation of this theory.

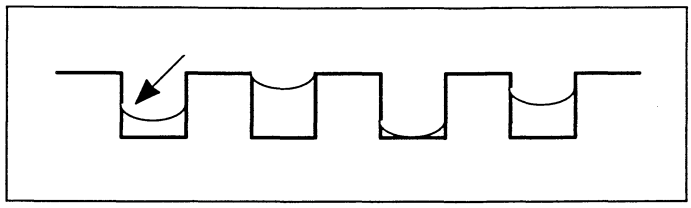

Fig. 4.23. Liquid settled irregular in the hole pattern.

Further, the shape of the liquid surface may have an influence on the ablation. Due to the surface tension, the liquid surface is not even. At least not close to a wall, see arrow Fig. 4.23.

As mentioned in the introduction (Ch 4.1), formation of fine bubbles during laser ablation of liquids has previous been observed. Moreover, for NaCl solutions the total gas yield, i.e. the integrated bubble volume, is found to increase with the concentration of the solution, i.e. with the absorption coefficient[40]. This is true also for these experiments. An exception is Tetracaine, which was found to have a relative high absorption coefficient, but a relative low bubble formation. To what extent the bubble formation influences the ablation is not clear.

The photos in Figures. 4.12 -20 show some interesting details:

The sharp edge shown in e.g. Fig 4.18 a for Dextran 7 % is very likely caused by the ablation threshold for PMMA.[46] This means that to ablate PMMA, a certain intensity is needed. If the intensity is lower than the needed one, no ablation take place.

The peaks for Dextran 7 % and Celluvisc in the profile curves (Figures 4.9 and 4.10), can also be seen on the photos (Figures 4.20 a and 4.18 b).

Even though Oxane looks smooth in the profile curves (Figures 4.9 and 4.10), the photos (Fig. 4.16) show otherwise.

4.5.2 Results

The results show that the hole pattern is not a well designed method to determinate the potential of the masking agents. The high significance for many liquids that nothing has changed, makes it difficult to conclude anything. What can be said is that without doubt, Healon and Oxane has an influence on the ablation process and that BSS, Tears Natural, Methocel, Celluvisc and Ophthalin most likely also effect the ablation. For Perfluorooctane, the measured difference between tops and bottoms is larger after the ablation. Therefore the values in the "Difference"-column in table 4.3 is negative for this liquid. The reason for the uncertainty (the large confidence interval) in the results from the hole patterns, may, besides bad application, be the shape of the bottoms of the holes. The conical shape, see Fig. 4.10, makes it difficult to average the values.

The results for the square patterns, table 4.2, are more interesting. Here the zero-hypothesis for dist. water BSS, Methocel, Celluvisc, Ophthalin and Oxane is rejected at the 0.1 % significance level, which means that they without doubt influence the ablation process. For Healon, Tetracaine and Dextran 7 % , the high significance is due to the form of the profile curves. The differences between tops and bottoms for the ablated part, vary a lot. The confidence interval in

[46] Kueper S, p.11.

the "After"- column is therefore high, which gives a high level of significance. Hence, the three above mention liquids most likely prevent the PMMA disc better from the laser radiation than the results show, i.e. the differences listed are to low. Perfluorooctane has, for the square as well as for the hole pattern, a negative difference number. This may indicate that Perfluorooctane enhances the laser ablation.

4.5.3 Improvements

As a consequence of the results and this discussion, some improvements for the most grave problem with the used method are suggested:

The PMMA discs has to be even and have the same distances between tops and bottoms all over the surface. As can be seen in the "before" -column in table 4.2 and in the shape of Fig. 4.6 in Ch 4.3, this was not the case in these experiments and may have given rise to an error in the measurements.

The material of the base (the disc), here PMMA, should be considered. The liquids capability of forming drops on the surface of the discs, make the results doubtful. Perhaps a new base material can solve this problem.

The reflection of the laser beam in the UBM instrument was sometime low, due to the transparency of the PMMA-discs. This could give rise to measurement errors. A thin gold layer on the surface of the PMMA disc or a new material should give better results.

If the statistical calculations were made with more samples, the results would naturally be more reliable

5. Final Discussion

5.1 Ablation vs. Absorption

This work has so far been concentrated on the optical and ablation properties of the liquids as two independent parts. However, there may be a connection between these two kind of properties. To check this, the attenuation coefficients at 193 nm (table 3.4, Ch. 3.4), as optical parameters, were plotted in fig 5.1 versus the difference between before and after ablation listed in table 4.2, Ch. 4.4.

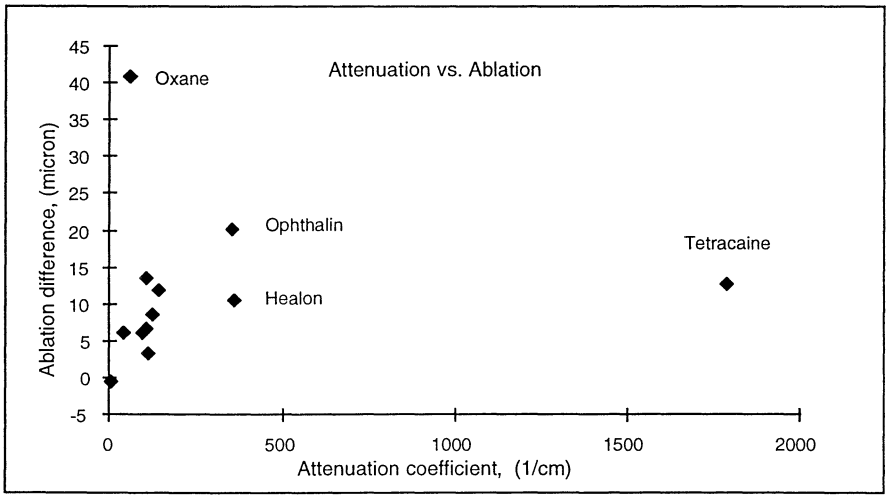

Fig. 5.1 Ablation difference vs. attenuation coefficient

A certain correlation can be observed for the two parameters, but the point for Oxane shows that the ablation is not determined only through the attenuation coefficient. As discussed in Ch. 4.1. it may also depend on other properties of the target, such as its reflectivity, density, specific heat, latent heat, temperature of melting and of the laser beam, such as repetition rate, energy per pulse and pulse length. Here, the laser parameters are the same for all liquids, but e.g. the reflectivity and the viscosity are different for different liquids. Interestingly, the refraction index for Oxane is significantly higher than for the other liquids used in the ablation experiment, see table 3.6, Ch 3.4.

Another reason could be that Oxane, like PMMA (see Ch. 4.1), changes the absorption coefficient due to UV - radiation. If this is the case, the correlation between the two parameters in Fig 5.1 may be better than it presently looks.

If the attenuation consists of a large scattering component, this may be a reason for bad correlation.

Even though also Tetracaine diverge significantly from the trend, this must not mean anything, but may be caused by the difficulties to apply this liquid to the PMMA-discs.

All the masking agents, except Tetracaine, has a very low attenuation at 213 nm compared to the attenuation at 193 nm. If there is a correlation between the attenuation and the ablation, this may imply that these masking agents do not very well stop the laser beam from reaching the underlying material at 213 nm. They will, in other words, be no good masking agents at 213 nm. Tetracaine, however, may be a good masking agent also for the 5f-Nd:YAG -laser at 213 nm.

5.2 In view of PTK

In this work, the liquids has been applied to a disc of PMMA. This disc has worked as a model of the cornea. The pattern on the disc surface has functioned as a model of the irregularities in and on the cornea, treated in PTK.

The ablation properties for PMMA are, however, not the same as for the cornea. The 193 nm ArF excimer laser has previous been observed to have an ablation rate in cornea of 0.24 - 0.28 µm / pulse [47] The ablation rate for the used PMMA - discs were found to be 35 - 45 µm / 320 pulses. If each pulse can be assumed to have the same ablation rate, this equals 0.11 - 0.15 µm / pulse. Yet, for ablation at 248 nm, the PMMA has been found to need some incubation pulses, to be ablatable.[48] The incubation pulses change the chemical composition of the PMMA, which give rise to an higher absorption in the material. This is possible true also at 193 nm, why the ablation rate may be higher than the above calculated.

As discussed in Ch 4.1, the ablation may be enhanced if tissue is anyway constrained. The masking agents constrains to some extent the cornea. Hence, the ablation of the cornea may diverge from that of the PMMA - disc. Furthermore, the threshold intensity may differ between PMMA and cornea, giving rise to unexpected results for the latter one.

These findings implies that from the results of the ablation of the PMMA - discs, no quite secure conclusions can be drawn about the ablation of the cornea and the ablation rate of the liquid. Still, if the ablation process is assumed to be the same and the ablation rate of PMMA is assumed to be half as high as the same for the cornea, the ablation rate of the liquids can to some extent be judged.

The PMMA - disc was ablated with 320 pulses, what equals approximately 80 µm in cornea or around 40 µm in PMMA. For the ca. 40 µm deep patterns of the PMMA - discs, this means that if the patterns are ca. 20 µm deep after the ablation, the masking agent has the same ablation rate as the cornea. For the values listed in the "differences" column in table 4.2 in Ch. 4.4 this equals ca. 20 µm.

---

[47] Stevens SX and Bowyer BL, Corneal modulators and their use in excimer laser PTK, *Int. Ophtalmology Clinics*, **36**,119-125,1996
[48] Kueper. S, 10-11

Closest to 20 μm for the square pattern is Celluvisc, Methocel, Healon, Ophthalin and Tetracaine. For the hole pattern just Healon is close to the ideal. Oxane can possibly be used if the radiation are to be almost complete stopped. Though, the photos of Oxane show a very irregular ablated surface (fig. 4.16)

The attenuation coefficient of the cornea at 193 nm has previous been determined to 2340 ± 450 cm^{-1}. [49] The highest attenuation coefficient for the tested masking agents at 193 nm is 1790 ± 60 for Tetracaine but the second highest is just 360 ± 117 for Healon. Oxane, with the highest capability of stopping laser beams, has an even lower attenuation coefficient. This implies that the attenuation coefficient does not have to be the same as for the cornea for a good masking agent.

5.3 Previous Works

In two previous work, masking agents has been investigated.

The first by E.W. Kornmehl et al.[50] compared three different masking agents: Tears Natural, Celluvisc and Unisol. The experiments were accomplished on calf-eyes, with 500 pulses ablation, a repetition rate of 10 Hz and a fluence of 180 mJ / cm^2. The exposure disc was 4 mm in diameter. A model of an irregular anterior corneal surface, was developed with a sandpaper. Tears Natural was found to give " Mild " surface irregularities, the two other "Moderate".

The second by T.D. Fitzsimmons and P Fagerholm[51] investigated three different liquids as well: Tetracaine, Methocel and Healon-Yellow, a fluorescein containing hyaluronate preparation. The masking agents were applied to corneas of anesthetized rabbits. Over the corneas a copper grid had been placed and a pattern had been etched into the cornea with the 193 nm excimer laser. The nominal depth was 40 μm and the beam width 2.5 mm. From the three investigated liquids, Tetracaine was found to give the smoothest surface. The other gave a "somewhat more uneven topography".

Due to the lack on an absolute determination of the ablation parameters, it is difficult to compare these results with them of this work.

[49] Lembares A., Far ultraviolet absorption spectra of porcine and human corneas, *SPIE*, **2971**, 46-54, 1997
[50] Kornmehl EW, 1991
[51] Fagerholm P., Fitzsimmons T.D, 1991

6. Conclusions

6.1 Absorption and Scattering

6.1.1 Method

Measurement of the attenuation for a liquid in a spectrophotometer in the far UV-region, is possible but may give rise to problem. The accuracy and repeatability of the used dual beam spectrophotometer deteriorated in the region around and below 200nm. Above all the stray-light was found to have a large influence at short wavelengths. To improve the accuracy with respect to the stray-light, a filter which stops light of other frequencies than far UV-light, can be used. Another possible method is to use double or triple monochromators, though this will strongly reduce the intensity of the radiation. Moreover, the slit width / Spectral Band Width (SBW) was found to be important for the results. A SBW of 1 nm instead of the used 2 nm, would give more accurate results.

To measure the diffuse absorption in the far UV-region with an integrating sphere coated with Spectralon, showed to be difficult. The light intensity from the deuterium lamp was found to be weak in the region below 250 nm. Together with the low reflectance for the Spectralon coating, this made the measurements inaccurate in the far UV-region.

The external fibre optic path used to measure the angle dependence of the scattering, gave no reliable results in the far UV region. The light source (a deuterium lamp) has to be stronger or the detector more sensitive.

6.1.2 Results

All the measured absorbance spectra, except Tetracaine and DDS, show a spectrum with a relatively low attenuation for visual light and a strongly increasing attenuation around 200 nm. Tetracaine, however, has a broad attenuation peak around 320 and a strong increase of the attenuation already around 250 nm. For DDS, the spectrum has an increasing attenuation already at ca. 280 nm. This makes the attenuation for DDS too high at 193 and 213 nm to be measured with the available QS-cells.

The absorbance is for the longest cell (0.02 cm) at 193 nm not a linear function of the pathlength. This is probably mainly due to the straylight. Therefore the attenuation coefficient calculated from the three shortest pathlengths is probably the most correct at 193 nm. However at 213 nm, where the straylight has less influence, the attenuation coefficients calculated from all four pathlengths are probably most correct.

The scattering was, with available instruments, impossible to measure for the far UV-region. Therefore it can not be told in what extent the measured attenuation is scattering.

6.2 Laser Ablation

6.2.1 Method

The method chosen to measure the ablation of the masking agents, with two different patterns on PMMA-discs, was usable but had some imperfections.

The liquids were difficult to apply to the discs (above all Dextran 7 % and 15 %). This may be improved if another material, instead of PMMA, is used as material for the discs. Another pattern could also be helpful.

The shape of the discs and the patterns were unsatisfactory. The discs were not plane and the distances from tops to bottoms in the patterns were not all over the same. This may be improved with a better production method. One possibility is to produce them with the excimer laser. A (copper) grid could be placed over the PMMA disc after which the pattern is etched into the disc with an excimer laser.

From the two tested pattern, the square pattern was found to be the best suited.

6.2.2 Results

The liquids may, due to the results and the discussion (Ch. 4.5) be classified into five groups:

1	Perfluorooctane
2	Perfluorodecaline, Dest. water, NaCl 0.9 %, BSS, Tears Natural
3	Methocel, Celluvisc, (Healon, Tetracaine)
4	Ophthalin, (Healon, Tetracaine)
5	Oxane

Table 6.1 The liquids classified after capability to stop the laser radiation. Group 4 contains the most preventing liquid.

The groups are arranged after increasing capability of stopping laser radiation. The two Dextran solutions are not placed in the table, due to lack of reliable results.

6.3 Attenuation and Ablation

No direct connection was found between the ablation rate and the attenuation coefficient of the tested masking agents. This is probably due to the influence on the ablation rate from other parameters, such as the reflectivity and viscosity.

If the ablation results are discussed in the view of PTK, the masking agents with the ablation rate closest to the same of the cornea seems to be: Ophthalin, Healon, Methocel and Celluvisc. Oxane has probably a lower ablation rate than the cornea.

7. Future Developments

This work is a part of the work to find a masking agent, which gives a smooth surface to the cornea. For this purpose, not just the ablation properties of the masking agent is interesting. Steven and Bowyer[48] established following properties as desirable for a ideal masking agent.

- Non-toxic and biocompatible, i.e. causes no reaction at the cornea or at any other tissue in contact with the liquid.
- Distinguishable from corneal tissue to faciliate monitoring of the ablation.
- When applied, viscosity adequate to fill corneal irregularities homogeneously.
- Excellent corneal surface adherence with no movement due to beam pressure.
- Capable of moulding to any desired curvature.
- Easy manipulation and removal
- Ablation parameters, similar to them of the cornea.

Perhaps cheap should be added ?

All these properties has to be optimised at the same time, what requires a lot of work and experiments direct with corneas as a complement to PMMA investigations.

Due to the possible influence from the threshold intensity, the incubation pulses or the liquids confinement of the water vapour (see Ch. 5), it would be interesting to see if ablation of a liquid on PMMA, gives the same result as a liquid on cornea.

Further, to determine the ablation rate with our pattern method accurate, measurements has to be made for pattern with different deeps, not just 40 μm, as in this work.

To check the correlation between ablation and absorption more accurately, the influence of the UV-light and the scattering on the attenuation coefficients, should be investigated.

The influence of the laser beam parameters on the ablation rate, is another field of interest. Especially the pulse frequency may be important. Fasano et al.[52] suggested a low repetition rate, as this allows the liquid two flow over the surface and fill all the irregularities.

Finally, it would be of interest to quantify the ablation of the masking agents with the 5f-Nd:YAG - laser at 213 nm. In addition this would allow a comparison with the attenuation coefficients at 213 nm determined in this work.

---

[52] Fasano AP, Moreira H, McDonnell PJ, et al., Excimer laser smoothing of a reproducible model of anterior corneal surface irregularities, *Ophtamology*, **98**, 1782-1785, 1991

8. Acknowledgements

Primarily I would like to thank my supervisor in Switzerland at ETH Dr. Pascal Rol for his helpful and humorous supervision of my work. Secondly I would like to thank Dr. Stefan Andersson-Engels for his great help with the examination here in Sweden. I would also like to thank all the other professors, doctors and assistants, working at the Institute of Biomedical Technology in Zuerich, that has helped me with various problems. Finally, a special thank to Dr. Eduard Häfflinger in Basel and Dr. Volkert Ziebart in Zuerich for making important instruments available to me. Thank You !

9. References

9.1 Books and Papers

Bergman, Schaefer, Lehrbuch der Experimentalphysik, Band 3 (Optik), Walter de Gruyter, 1989

Burgess C.and Knowles A, Standards in Absorption Spectrometry (Ultraviolett Spectrometry Group), Chapman and Hall, London, 95-99, 1981

Christopher JR, Excimer laser phototherapeutic keratectomy, *Int. Ophtalmology Clinics*, **36,**127-136,1996

Deutsch, TF, IR-Laser Ablation in Medicine: Mechanism & Applications,*Lecture Notes in Physics,* **389**, Springer Verlag, Berlin-Heidelberg, p.111, 1991

Dimitri TA, et al., Phototherapeutic keratectomy, the VISX Experience, *Corneal Laser Surgery*, , p.213-226

Fagerholm P., Fitzsimmons T.D., Superficial keratectomy with the 193 nm excimer laser, *Acta Ophthalmologica,* **69**, 641-644, 1991.

Fantes FE, Hanna KH, Waring III GO, et al., Wound healing after excimer laser lamellar keratectomy, *Ophtamology,* **96**, 654-664, 1989

Fasano AP, Moreira H, McDonnell PJ, et al., Excimer laser smoothing of a reproducible model of anterior corneal surface irregularities, *Ophtamology*, **98**, 1782-1785, 1991

Goddard D. A., The Cleaning of vitreous silica cells, *UV Spectrometry Group Bulletin*, **4,** 19, 1976

Ishimaru A, Wave Propagation and Scattering, London, 814-815, 1991

Kornmehl EW, et al., A comparative study of masking fluids for excimer laser PTK, *Arch Ophtalmol*, **109**, 860-863, 1991

Kreyszig E., Statistische Methoden und ihre Anwendungen, Vadenhoeck & Ruprecht, Goettingen, 270 - 271 & 300 - 301, 1979

Kueper S., Ablation mit UV-Laserlicht (Dissertation), Goettingen, 20-46

van Leeuwen TG, et al., Pulsed Laser Ablation of Soft Tissue, *Optical Thermal Response of Laser Irradiated Tissue,* Plenum Press, New York, 709-711, 1995

Lembares A., Far ultraviolet absorption spectra of porcine and human corneas, *SPIE*, **2971**, 46-54, 1997

Meister E., Spectrophotometri, Instruktion fuer Physikalisch Chemisches Praktikum 1,1997

Sommer L., Analytical Absorption Spectrophotometry in the visible and the UV - The Principles, (Studies in Analytical Chemistry) , Elsevier, Amsterdam, p.13, 1989.

Stark WJ,Chamon W, Kamp MT et al., Clinical follow up 193 nm ArF excimer laser photokeratectomy, *Ophtalmology* , **99**, 805-811,1983

Stevens SX and Bowyer BL, Corneal modulators and their use in excimer laser PTK, *Int. Ophtalmology Clinics*, **36,**119-125,1996

Svanberg S, Atomic and Molecular Spectroscopy, Springer Verlag, Berlin-Heidelberg,, 56-60, 1992.

Svehla G., Comprehensive Analytical Chemistry, **4,** Elsevier, Amsterdam, p.69, 1975

Torkel SL, Srinivasan R, Braren B, Excimer laser surgery of the cornea, *Am J Ophtalmol,* **96**, 715-720, 1983.

Turovets L et. al., ArF Excimer laser induced bubble formation during irradiation of NaCl solutions, *Photochemistry & Photobiology,* **60** No. 5, 1994

Walsh JT Jr., Pulsed CO_2 Laser ablation of tissue, effect of mechanical properties, *IEEE Trans. Biomed. Eng.,* **36**, 1195-1201, 1990

9.2 Instruction Manuals

Hellma, Kuvetten-Eigenschaften, Hellma GmbH, Germany.

Labsphere, Instruction manual for RSA-SZ-1601,1989

Newport Corporation, Model 835 Operating Manual, Newport Corporation, Fountain Valley, U.S.A, 1987.

Perkin-Elmer Lamba 6, User manual.

Shimadzu UV-1601, Instruction Manual, Shimadzu Corp.

Technolas GMBH, Keracor 116, Excimer laser for corneal surgery, Instruction manual

Abbe Refractometer, Carl Zeiss, Instruction Manual.

For four interfaces, like in fig. A.3, the transmission - matrix is derived to be:

$$\mathbf{I_B} = \mathbf{R}\cdot\mathbf{R}\cdot\mathbf{R}\cdot\mathbf{R}\cdot\mathbf{I_A} = \mathbf{R}_C\cdot\mathbf{I_A} = \frac{1}{1-R}\begin{pmatrix} 1-5R & 4R \\ -4R & 1+3R \end{pmatrix}\cdot\mathbf{I_A} \qquad \text{(A.9)}$$

$\mathbf{I_B}$ and $\mathbf{I_A}$ are defined as in Fig. A.3 below.

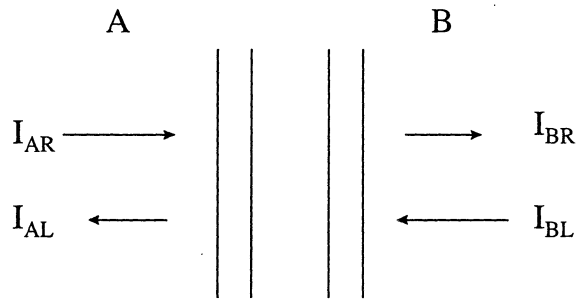

Figure A.3. Four interfaces.

If now, as for two interfaces, I_{BL} is assumed to vanish, the transmittance through all interfaces, T_C can be expressed as:

$$T_C = \frac{I_{BR}}{I_{AR}} = \frac{1-R}{1+3R} \qquad \text{(A.10)}$$

and the reflectance, R_C, as:

$$R_C = \frac{I_{AL}}{I_{AR}} = \frac{4R}{1+3R} \qquad \text{(A.11)}$$

In the next step the space between the two innermost interfaces is assumed to be absorbing. Therefore a new matrix, describing the absorption, is derived.

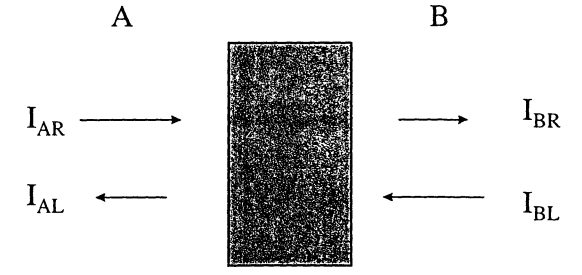

Figure A.4. Absorption between two interfaces

With notations according to Fig. A.4 the equations for the absorption become:

$$I_{BR} = e^{-\mu L} I_{AR} \tag{A.12}$$

$$I_{BL} = e^{\mu L} I_{AL} \tag{A.13}$$

and the matrix:

$$\mathbf{I_B} = \begin{pmatrix} e^{-\mu L} & 0 \\ 0 & e^{\mu L} \end{pmatrix} \cdot \mathbf{I_A} = \mathbf{A} \cdot \mathbf{I_A} \tag{A.14}$$

If now the outermost and innermost interfaces are assumed to have different reflection, R_0 and R_1, the transmittance through the interfaces in Fig. A.5 can be calculated with simple matrix multiplication.

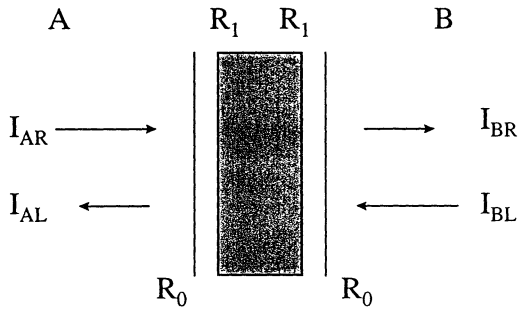

Figure A.5. Four interfaces, were the medium between the innermost interfaces absorbs a part of the radiation.

$$\mathbf{I_B} = \mathbf{R_0} \cdot \mathbf{R_1} \cdot \mathbf{A} \cdot \mathbf{R_1} \cdot \mathbf{R_0} \cdot \mathbf{I_A} = \mathbf{R_{FC}} \cdot \mathbf{I_A} \tag{A.15}$$

Here the matrices R_0 and R_1 are identical with the matrix R, except for the index. From the matrix $\mathbf{R_{FC}}$ the transmission, T_{FC}, may as usual be calculated under the assumption that I_{BL} is vanishing:

$$T_{FC} = \frac{I_{BR}}{I_{AR}} = \frac{(1-R_0)^2 (1-R_1)^2 e^{-\mu L}}{(1-R_0 R_1)^2 - (R_1 + R_0 - 2R_1 R_0)^2 e^{-2\mu L}} \tag{A.16}$$